AKUSTICKÉ LISTY

České akustické společnosti
www.czakustika.cz

ročník 20, číslo 3–4 prosinec 2014

Obsah

ČESKÁ AKUSTICKÁ SPOLEČNOST

Rada České akustické společnosti svolává ve smyslu stanov

VALNOU HROMADU,

která se bude konat ve čtvrtek 22. ledna 2015 na Fakultě elektrotechnické ČVUT, Technická 2, Praha 6 – Dejvice.

Rámcový program:
13.00–13.45 Jednání v odborných skupinách. Rozpis místností pro jednání v odborných skupinách bude vyvěšen ve vstupním prostoru fakulty a na dveřích sekretariátu, místnost č. T2:B2-47.
13.45–14.15 Prezentace.
14.15–16.00 Plenární zasedání, místnost č. T2:C2-82.

Člen společnosti, který se nebude moci Valné hromady osobně zúčastnit, pověří jiného člena, aby jej zastupoval. Formulář zvláštní plné moci a oficiální pozvánka jsou součástí tohoto čísla Akustických listů. Současně jsou tyto dokumenty vystaveny na webové stránce ČsAS `http://www.czakustika.cz`.

Důležité upozornění: Tato zvláštní plná moc musí být předaná před začátkem Schůze osobně, nebo poštou. **Není možné akceptovat elektronickou verzi, a to ani oskenovanou kopii.** Podpis však nemusí být ověřený.

New Simplified Method for Estimating the Flanking Airborne and Impact Sound Transmission between Rooms in Residential Buildings

Nový zjednodušený způsob odhadu bočního přenosu zvuku a kročejového zvuku mezi místnostmi v obytných budovách

Jiří Nováček

CTU – FCE, Thákurova 7, 166 29 Praha 6
CTU – UCEEB, Třinecká 1024, 273 43 Buštěhrad

The introduction to new simplified method for estimating the apparent weighted sound reduction index and weighted normalized impact sound pressure level in residential buildings is done in this paper. This new method is based on prediction calculation models described in ČSN EN 12354 parts 1 and 2. Compared to these models the new method is significantly easier to use in daily practice without professional software. Corrections to flanking sound and impact sound transmission are determined from simple formula using partial theoretical corrections for various types of junctions between building elements. The early experience indicates that the new method gives similar results to those from standardized ČSN EN models and more general than empirical corrections described in ČSN 73 0532.

1. Introduction

Several methods were derived for the prediction of flanking sound transmission between rooms in past decades. Some of them are simplified models based on the use of single-number quantities or empirical corrections for flanking paths (e.g. Vrána, J. [6], Homb et al. [8], DIN 4109 [10]). Other methods like ČSN EN 12354 models allow detailed estimations of sound insulation quantities in frequency bands. These models are based on Gerretsen's work [7] from 70's and 80's and are suitable pro heavyweight buildings constructions. In the last years, there is a big effort to improve and validate them also for lightweight structures. For example, a complete theory for sound transmission has been described by J. H. Rindel [9].

Within the design stage of a construction process, the technical standard ČSN 73 0532 [1] recommends to use measured or calculated laboratory values of weighted sound reduction index R_w, corrected to in-situ quantity R'_w according to following formula

$$R'_\mathrm{w} = R_\mathrm{w} - k_1 \,, \tag{1}$$

where k_1 is the correction factor for flanking sound transmission. Basic value of $k_1 = 2$ dB is valid for partitions in buildings with massive walls and slabs. In buildings with columns this correction factor is higher, $k_1 = 2$ to 5 dB (for heavyweight partitions) or $k_2 = 4$ to 8 dB (for lightweight partitions). In some cases (e.g. buildings with difficult floor plans) it is recommended to determine this correction factor more precisely, for example using ČSN EN 12354-1 [2] prediction calculation models (detailed or simplified).

The prediction models described in ČSN EN 12354-1 are based on the general formula which defines the total sound power transmitted between two adjacent rooms in a building as a sum of the direct sound transmission through the common partition and the sound transmitted via flanking elements (floor, ceiling, side walls). Hence, the apparent sound reduction index R' is defined as follows

$$\begin{aligned} R' &= 10\lg\frac{W_0}{W_\mathrm{t,d} + \sum W_{\mathrm{t},ij}} \\ &= -10\lg\left(10^{-R/10} + \sum 10^{-R_{ij}/10}\right) \,, \end{aligned} \tag{2}$$

where W_0 is the incident sound power, $W_\mathrm{t,d}$ is the sound power transmitted via direct transmission path and $W_{\mathrm{t},ij}$ is the sound power transmitted via flanking path ij. Similarly, R is the sound reduction index for direct transmission a R_{ij} is the sound reduction index for flanking transmission path ij. Normally, 13 transmission paths are taken into account (one direct and three flanking paths through each of four junctions). Sound transmission from rear wall is neglected. The previous equation is also valid for single-number weighted quantities R'_w, R_w and $R_{\mathrm{w},ij}$.

In the detailed model, the sound reduction index R_{ij} for flanking sound transmission is given by following equation

$$R_{ij} = \frac{R_i + R_j}{2} + \frac{D_{v,ij} + D_{v,ji}}{2} + \Delta R_i + \Delta R_j + 10\lg\frac{S_\mathrm{s}}{\sqrt{S_i S_j}}, \tag{3}$$

where R_i, R_j is the sound reduction index of flanking element i or j respectively, term $(D_{v,ij} + D_{v,ji})/2$ is the direction-averaged junction velocity level difference, ΔR_i and ΔR_j is the sound reduction improvement index of

Přijato 10. srpna 2014, akceptováno 18. prosince 2014.

flanking element in source room or receiver room respectively, S_s is the surface area of common partition and S_i and S_j is the surface area of element i or j respectively.

In simplified model, the weighted sound reduction index $R_{\mathrm{w},ij}$ is defined as

$$R_{\mathrm{w},ij} = \frac{R_{\mathrm{w},i} + R_{\mathrm{w},j}}{2} + \Delta R_{\mathrm{w},ij} + K_{ij} + 10\lg\frac{S_\mathrm{s}}{l_0\, l_\mathrm{f}} \ , \quad (4)$$

where K_{ij} is the vibration reduction index, l_f is the common length of joint between separating element and flanking element and l_0 is the reference joint length (= 1 m).

The use of both of these models requires the knowledge of many acoustical properties of several building elements and junctions involved in the sound transmission path while the empirical approach of ČSN 73 0532 is simply based on the type of the building. This fact complicates the prediction process a lot. Here is a brief overview of required properties:

- sound reduction indexes and dimensions of all building elements (e.g. partition, facade, floor, ceiling),
- mounting conditions of all building elements,
- vibration attenuation characteristics of all structural junctions.

Acousticians rarely have such a complete information about the building situation for calculations. Moreover, the presence of windows, doors, multiple indoor partitions, etc., leads towards the need of model adaptation to real situation. This introduces other unpredictable human errors. The exclusion of these problems was the main motivation for the development of a new prediction method. Therefore this new method is simply based on the knowledge of a type and a surface mass of each building element and a type of each junction. Other acoustical and geometrical properties such as structural reverberation time, dimensions, etc., are excluded or the mean values are considered. This approach usually gives overestimated (safer) results.

Similarly to airborne sound, for impact sound transmission between rooms ČSN 73 0532 [1] recommends to use measured or calculated laboratory values of weighted normalized impact sound pressure levels $L_{\mathrm{n,w}}$, corrected to in-situ quantity $L'_{\mathrm{n,w}}$ according to following formula

$$L'_{\mathrm{n,w}} = L_{\mathrm{n,w}} + k_2 \ , \quad (5)$$

where k_2 is the correction factor for flanking impact sound transmission (normally $k_2 = 0$ dB to 2 dB). In some cases (e.g. buildings with difficult floor plans) it is recommended to determine this correction factor more precisely, for example using ČSN EN 12354-2 [3] prediction calculation models (detailed or simplified).

According to ČSN EN 12354-2 the total normalized impact sound pressure level L'_n is defined as energy sum of normalized impact sound pressure level L_n caused by direct transmission and normalized impact sound pressure levels $L_{\mathrm{n},ij}$ caused by flanking transmission

$$L'_\mathrm{n} = 10\lg\left(10^{L_\mathrm{n}/10} + \sum 10^{L_{\mathrm{n},ij}/10}\right) \ . \quad (6)$$

In special case of horizontal direction of propagation of impact sound (i.e. two rooms which are next to each other) this equation is reduced to flanking transmission only

$$L'_\mathrm{n} = 10\lg\left(\sum 10^{L_{\mathrm{n},ij}/10}\right) \ . \quad (7)$$

Four flanking transmission paths for vertical and two for horizontal direction of propagation are usually taken into account.

In the detailed model, the normalized impact sound pressure level caused by flanking transmission is given by following equation

$$L_{\mathrm{n},ij} = L_{\mathrm{n,slab}} - \Delta L_\mathrm{n} + \frac{R_i - R_j}{2} - D_{v,ij} - \Delta R_j - 10\lg\sqrt{\frac{S_i}{S_j}} \ , \quad (8)$$

where R_i is the sound reduction index of excited (separating) building element i, R_j is the sound reduction index of flanking element j, $D_{v,ij}$ is the junction velocity level difference for impact sound transmission from element i to element j, ΔR_j is the sound reduction improvement index of flanking element in receiver room, S_i is the surface area of excited (separating) element and S_j is the surface area of flanking element j in receiver room.

The prediction of weighted normalized impact sound pressure level $L'_{\mathrm{n,w}}$ according to simplified model is based on following general formula

$$L'_{\mathrm{n,w}} = L_{\mathrm{n,w}} - \Delta L_\mathrm{w} + K \ , \quad (9)$$

where $L_{\mathrm{n,w}}$ is the weighted normalized impact sound pressure level of a slab, ΔL_w is the reduction of weighted normalized impact sound pressure level caused by floor construction and K is the correction factor for flanking transmission. This factor K is given in a table form in ČSN EN 12354-2 and depends on the mean surface mass of all flanking elements and the surface mass of separating element.

The motivation for the development of new prediction method was the same to those for airborne sound transmission. It must be said that the new method is finally similar to the simplified model described in ČSN EN 12354-2 which is also based on tabular corrections for flanking transmission. However, these corrections are considered individually for each junction in the new method, whereas in ČSN EN model they depend on mean surface mass of all flanking elements. Hence, the new method is more correct and accurate in general.

2. New method for estimating the apparent weighted sound reduction index

According to the new proposed method the apparent weighted sound reduction index R'_{w} is calculated from the similar equation as that written in ČSN 73 0532

$$R'_{\mathrm{w}} = R_{\mathrm{w}} - k_{\mathrm{air}} \ , \tag{10}$$

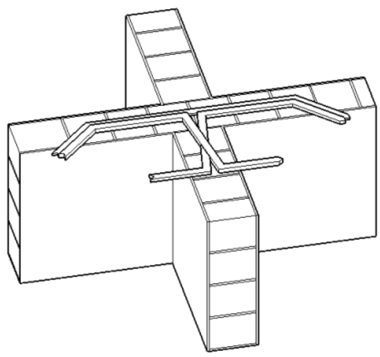

m'_{f} (kg·m^{-2})	k_i (dB) m'_{d} (kg·m^{-2}) 100	200	300	400	500	600
100	0.6	1.2	2.0	2.6	3.2	3.7
200	0.2	0.6	1.2	1.8	2.3	2.8
300	0.1	0.3	0.6	1.0	1.4	1.8
400	0.0	0.1	0.3	0.6	0.9	1.2
500	0.0	0.1	0.2	0.4	0.6	0.8
600	0.0	0.1	0.1	0.3	0.4	0.6

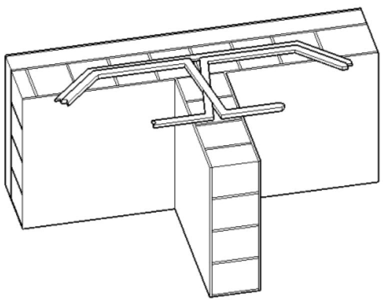

m'_{f} (kg·m^{-2})	k_i (dB) m'_{d} (kg·m^{-2}) 100	200	300	400	500	600
100	1.1	2.2	3.6	4.7	5.6	6.3
200	0.4	1.1	2.2	3.2	4.1	4.9
300	0.2	0.5	1.1	1.8	2.5	3.2
400	0.1	0.3	0.6	1.1	1.6	2.2
500	0.0	0.2	0.4	0.7	1.1	1.5
600	0.0	0.1	0.3	0.5	0.8	1.1

Figure 1: Corrections k_i of weighted apparent sound reduction index R_{w} for flanking sound transmission [4]

where k_{air} is the correction factor for flanking sound transmission ($\approx\ k_1$ in ČSN 73 0532). This factor is calculated from following equation

$$k_{\mathrm{air}} = 10\lg\left[(1-n) + \sum 10^{k_i/10}\right] \ , \tag{11}$$

where n is the number of flanking elements connected to separating partition and k_i is the correction factor of weighted laboratory sound reduction index R_{w} caused by the presence of flanking element i. Normally $n = 4$ and $k_1, \ldots, k_4$ are correction factors for sound transmission via floor, ceiling and two side walls. These factors have been calculated using simplified model from ČSN EN 12354-1 for different types and surface masses of flanking elements and different types of junctions. For easier use the results have been tabelized (see next two examples for rigid X- and T-junctions and heavyweight building elements). In both tables, m'_{d} is the surface mass of separating element (perpendicular to the direction of propagation) and m'_{f} is the surface mass of flanking element (parallel to the direction of propagation).

More tables with correction factors for other junctions and elements can be found in the final report of COST CZ project No. LD12075 "Effective design of sound insulating constructions in buildings" [4].

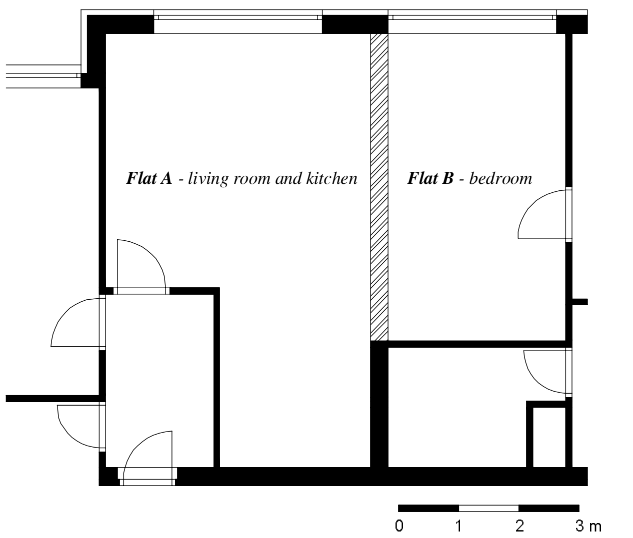

Figure 2: Floor plan for prediction of airborne sound insulation between rooms [5]

Model example Calculate the weighted apparent sound reduction index between two rooms in Figure 2. The separating wall between flats is a heavyweight block wall 300 mm thick with surface mass $m'_{\mathrm{d}} = 345\,\mathrm{kg{\cdot}m^{-2}}$. The floor consists of a concrete slab with surface mass $615\,\mathrm{kg{\cdot}m^{-2}}$ and a heavyweight floating floor. Indoor masonry partitions are $85\,\mathrm{kg{\cdot}m^{-2}}$ and the facade wall is $300\,\mathrm{kg{\cdot}m^{-2}}$.

Direct transmission ($m'_\mathrm{d} = 345\,\mathrm{kg{\cdot}m^{-2}}$):

$$R_\mathrm{w} = 56 \text{ dB}$$

Flanking transmission:
No. 1 (T-juction, $m'_{\mathrm{f}_1} = 300$ kg·m^{-2}): $k_1 = 1.5$ dB
No. 2 (X-junction, $m'_{\mathrm{f}_2} = 615$ kg·m^{-2}): $k_2 = 0.2$ dB
No. 3 (T-junction, $m'_{\mathrm{f}_3} = (345 + 85)/2 = 215$ kg·m^{-2}): $k_3 = 2.7$ dB
No. 4 (X-juction, $m'_{\mathrm{f}_4} = 615$ kg·m^{-2}): $k_4 = 0.1$ dB

$$k_\mathrm{air} = 10\lg(-3 + 10^{0.15} + 10^{0.02} + 10^{0.27} + 10^{0.01}) = 3.7 \text{ dB}$$

Total transmission:

$$R'_\mathrm{w} = 56 - 4 = 52 \text{ dB}$$

The difference in the approach of the new method and the prediction models described in ČSN EN 12354-1 is illustrated in Figure 3. In the ČSN EN models three flanking paths are studied separately for each junction – $(\mathrm{F}_i, \mathrm{d})$, $(\mathrm{D}, \mathrm{f}_i)$ a $(\mathrm{F}_i, \mathrm{f}_i)$, while in the new method all these paths are considered together introducing one correction factor k_i for each junction.

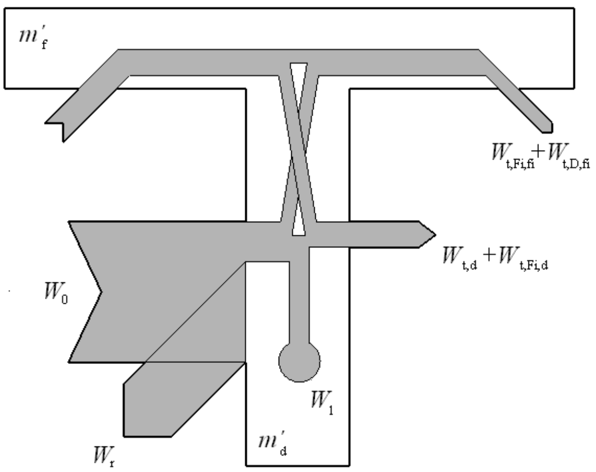

Figure 3: Direct and flanking airborne sound transmission through one structural junction

The general formula for the direct sound reduction index is

$$R = -10\lg\frac{W_\mathrm{t,d}}{W_0}\ , \tag{12}$$

where $W_\mathrm{t,d}$ is the sound power transmitted via direct path and W_0 is the sound power incident on the separating element. The flanking sound reduction index for each of four junctions is given by following equation

$$\begin{aligned} R_i &= -10\lg\left(\frac{W_{\mathrm{t,F}_i\mathrm{,d}} + W_{\mathrm{t,F}_i\mathrm{,f}_i} + W_{\mathrm{t,D,f}_i}}{W_0}\right) \\ &= -10\lg\left(10^{-R_{\mathrm{F}_i\mathrm{,d}}/10} + 10^{-R_{\mathrm{F}_i\mathrm{,f}_i}/10} + 10^{-R_{\mathrm{D,f}_i}/10}\right)\ . \end{aligned} \tag{13}$$

For the explanation of all above mentioned sound power quantities see Figure 3. The apparent sound reduction index for sound transmission between two rooms via direct path and one flanking path through junction „i“ can be written as

$$\begin{aligned} R'_i &= -10\lg\left(\frac{W_\mathrm{t,d} + W_{\mathrm{t,F}_i\mathrm{,d}} + W_{\mathrm{t,F}_i\mathrm{,f}_i} + W_{\mathrm{t,D,f}_i}}{W_0}\right) \\ &= -10\lg\left(10^{-R/10} + 10^{-R_i/10}\right)\ . \end{aligned} \tag{14}$$

Considering weighted quantities the previous equation can be re-written to following form

$$R'_{\mathrm{w},i} = -10\lg\left(10^{-R_\mathrm{w}/10} + 10^{-R_{\mathrm{w},i}/10}\right)\ . \tag{15}$$

The correction factor k_i defined as a degradation of the weighted laboratory sound reduction index of separating element R_w caused by the presence of one flanking element (junction) i is then

$$k_i = R_\mathrm{w} - R'_{\mathrm{w},i}\ . \tag{16}$$

By adding this relationship to the previous equation we obtain the formula for weighted sound reduction index for flanking path (element) i

$$\begin{aligned} R_{\mathrm{w},i} &= -10\lg\left(10^{-R'_{\mathrm{w},i}/10} - 10^{-R_\mathrm{w}/10}\right) \\ &= -10\lg\left(10^{-(R_\mathrm{w}-k_i)/10} - 10^{-R_\mathrm{w}/10}\right)\ . \end{aligned} \tag{17}$$

This equation can be combined with the general formula for apparent weighted sound reduction index. For n junctions between separating element and flanking elements (normally 4 junctions) we obtain the final formula for flanking correction factor k_air

$$R'_\mathrm{w} = R_\mathrm{w} - k_\mathrm{air} = R_\mathrm{w} - 10\log\left[(1-n) + \sum 10^{k_i/10}\right]\ . \tag{18}$$

3. New method for estimating the weighted impact sound pressure level

According to the new proposed method the weighted normalized impact sound pressure level $L'_\mathrm{n,w}$ is calculated from the similar equation to that written in ČSN 73 0532

$$L'_\mathrm{n,w} = L_\mathrm{n,w} + k_\mathrm{imp}\ , \tag{19}$$

where k_imp is the correction factor for flanking impact sound transmission ($\approx k_2$ in ČSN 73 0532). This factor is calculated from following equation

$$k_\mathrm{imp} = 10\lg\left[(1-n) + \sum 10^{k_i/10}\right]\ , \tag{20}$$

where n is the number of flanking elements connected to excited floor and k_i is the correction factor of weighted normalized impact sound pressure level $L_{n,\mathrm{w}}$ of this floor caused by the presence of flanking element i (not the same as k_i for the airborne sound transmission). Normally $n = 4$ and $k_1, \dots, k_4$ are corrections for impact sound transmission via side walls. These factors have been calculated using detailed ČSN EN 12354-2 model for different types and surface masses of flanking elements and junctions. For easier use the results have been tabelized (see next two examples for rigid X- and T-junctions and heavyweight building elements). In both tables, m'_d is the surface mass of separating element (excited plate) and m'_f is the surface mass of flanking element (wall radiating sound to receiver room).

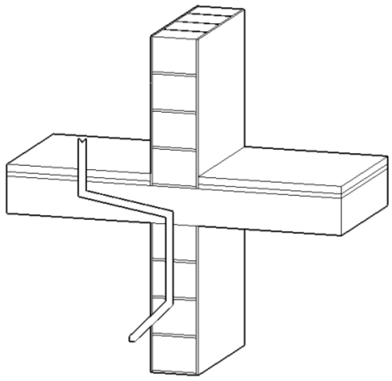

k_i (dB)						
m'_f	m'_d (kg·m^{-2})					
(kg·m^{-2})	100	200	300	400	500	600
100	0.2	0.5	0.8	1.1	1.4	1.6
200	0.1	0.2	0.4	0.6	0.9	1.1
300	0.0	0.1	0.2	0.	3 0.5	0.6
400	0.0	0.1	0.1	0.2	0.3	0.4
500	0.0	0.0	0.1	0.1	0.2	0.3
600	0.0	0.0	0.1	0.1	0.1	0.2

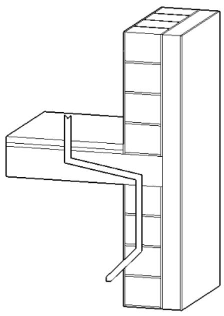

k_i (dB)						
m'_f	m'_d (kg·m^{-2})					
(kg·m^{-2})	100	200	300	400	500	600
100	0.4	0.9	1.5	2.0	2.4	2.8
200	0.1	0.4	0.8	1.2	1.6	2.0
300	0.1	0.2	0.4	0.7	0.9	1.2
400	0.0	0.1	0.2	0.4	0.6	0.8
500	0.0	0.1	0.2	0.3	0.4	0.6
600	0.0	0.0	0.1	0.2	0.3	0.4

Figure 4: Corrections k_i of weighted normalized impact sound pressure level $L_\mathrm{n,w}$ for flanking transmission [4]

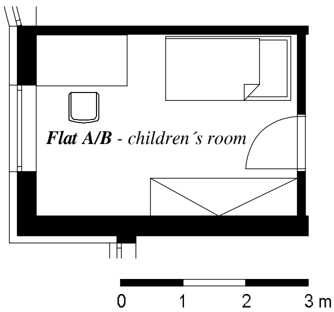

Figure 5: Floor plan for prediction of impact sound insulation between rooms [5]

Model example Calculate the weighted normalized impact sound pressure level of floor in room in Figure 5. The separating structure between flats is a heavyweight concrete slab 220 mm thick with a heavy floating floor. All side structures are masonry walls from hollow blocks.

Direct transmission ($m'_\mathrm{d} = 533$ kg·m^{-2}):

$$L_\mathrm{n,w} = 38 \text{ dB}$$

Flanking transmission:
No. 1 (T-junction, $m'_{\mathrm{f}_1} = 345$ kg·m^{-2}): $k_1 = 0.8$ dB
No. 2 (X-junction, $m'_{\mathrm{f}_2} = 134$ kg·m^{-2}): $k_2 = 1.2$ dB
No. 3 (X-junction, $m'_{\mathrm{f}_3} = 134$ kg·m^{-2}): $k_3 = 1.2$ dB
No. 4 (X-junction, $m'_{\mathrm{f}_4} = 345$ kg·m^{-2}): $k_4 = 0.4$ dB

$$k_\mathrm{imp} = 10\lg(-3+10^{0.08}+10^{0.12}+10^{0.12}+10^{0.04}) = 2.9 \text{ dB}$$

Total transmission:

$$L'_\mathrm{n,w} = 38 + 3 = 41 \text{ dB}$$

In the new method as well as in the detailed ČSN EN 12354-2 model one flanking path is considered for each junction – $(\mathrm{D}, \mathrm{f}_i)$ as shown in Figure 6.

The general formula for the normalized impact sound pressure level caused by the direct impact sound power transmission $W_{2,d}$ and the power transmission via one flanking path W_{2,f_i} is

$$\begin{aligned} L'_{\mathrm{n},i} &= 10\lg\left[\frac{4\rho_0 c_0 \left(W_\mathrm{2,d} + W_{2,\mathrm{f}_i}\right)}{p_0^2 A_0}\right] \\ &= 10\lg\left(10^{L_\mathrm{n}/10} + 10^{L_{\mathrm{n},i}/10}\right) \; . \end{aligned} \tag{21}$$

Considering weighted quantities the previous equation can be re-written to following form

$$L'_{\mathrm{n},i,\mathrm{w}} = 10\lg\left(10^{L_\mathrm{n,w}/10} + 10^{L_{\mathrm{n},i,\mathrm{w}}/10}\right) \; . \tag{22}$$

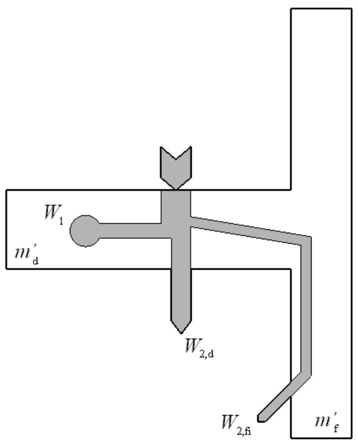

Figure 6: Direct and flanking impact sound transmission through one structural junction

The correction factor k_i defined as the increase of weighted laboratory normalized impact sound pressure level of separating element caused by the presence of one flanking element i is then

$$k_i = L'_{\mathrm{n},i,\mathrm{w}} - L_{\mathrm{n,w}} \,. \tag{23}$$

By adding this relationship to the previous equation we obtain the formula for weighted normalized impact sound pressure level caused by flanking path (element) i

$$\begin{aligned} L_{\mathrm{n},i,\mathrm{w}} &= 10 \lg \left(10^{L'_{\mathrm{n},i,\mathrm{w}}/10} - 10^{L_{\mathrm{n,w}}/10} \right) \\ &= 10 \lg \left(10^{L_{\mathrm{n,w}}+k_i/10} - 10^{L_{\mathrm{n,w}}/10} \right) \,. \end{aligned} \tag{24}$$

This equation can be combined with general formula for the normalized impact sound pressure level. For n junctions between separating element and flanking elements (normally 4 junctions) we obtain the final formula for flanking correction factor k_{imp}

$$L'_{\mathrm{n,w}} = L_{\mathrm{n,w}} + k_{\mathrm{imp}} = L_{\mathrm{n,w}} + 10 \lg \left[(1-n) + \sum 10^{k_i/10} \right] \,. \tag{25}$$

4. Conclusions

The proposed simplified method for estimating the apparent weighted sound reduction index and weighted normalized impact sound pressure level in residential buildings seems to be a useful prediction tool for the design stage of a construction process. It is more complex than the approach described in ČSN 730532 which is based on few empirical corrections and also easier to use than the calculation prediction models described in ČSN EN 12354-1 and -2. Although it is necessary to verify the accuracy of proposed simplified method in future, the first experiences on common situations indicate that the similar results can be expected to those from ČSN EN models. In more complex situations, especially if single heavyweight structures are combined with lightweight multilayered elements, the less accuracy is expected but towards the safer results.

Acknowledgements

This work has been supported by COST CZ 2012, grant No. LD12075 "Effective Design of Sound Insulating Partitions in Buildings", by internal grant project of CTU No. SGS13/108/OHK1/2T/11 and by European Union, project OP VaVpI No. CZ.1.05/2.1.00/03.0091 – University centre for energy efficient buildings.

References

[1] ČSN 73 0532 Acoustics – Protection against noise in buildings and evaluation of acoustic properties of building elements – Requirements (in Czech).

[2] ČSN EN 12354-1 (73 0512) Building acoustics – Estimation of acoustical performance of buildings from the performance of elements – Part 1: Airborne sound insulation between rooms.

[3] ČSN EN 12354-2 (73 0512) Building acoustics – Estimation of acoustical performance of buildings from the performance of elements – Part 2: Impact sound insulation between rooms.

[4] Nováček, J.: Effective design of sound insulating structures in buildings (in Czech), final report of grant project No. COST CZ LD 12075, FCE CTU in Prague, 2013.

[5] Nováček, J.: Calculation of airborne and impact sound insulation between rooms in residential buildings (in Czech), TZB info (on-line journal), ISSN 1801-4399, 2014, 16 (3).

[6] Zásady pro navrhování a posuzování konstrukcí a prostorů bytových a občanských staveb, Díl 1: Kritéria. Principy navrhování. Výpočtové metody. (in Czech) VÚPS Praha 1981, p. 193–202.

[7] Gerretsen, E.: Calculation of the Sound Transmission between Dwellings by Partitions and Flanking Structures, Applied Acoustics, 1979, 12(6).

[8] Homb, A., Hveem, S., Strøm, S.: Lydisolerenede konstruksjoner – Datasamling og beregningsmetode, Oslo, Norway: Norges byggforskninginstitut, 1983 (in Norwegian).

[9] Rindel, J. H.: Note 4214: Sound Insulation in Buildings – Tentative edition, Acoustic Technology, Ørsted DTU, 2004.

[10] DIN 4109 Beilblatt 1: 1989-11, Schallschutz im Hochbau; Ausführungsbeispiele und Rechenverfahren (in Deutsch).

Noise Measuring and Control on Industrial Fans

Měření a snižování hluku průmyslových ventilátorů

Tomáš Salava

VZLÚ, Beranových 130, 199 05 Praha

Following a brief introduction to noise problems in fans, contemporary methods and practices of fan noise measurements and evaluation are discussed. The principles and specific limitations of the use of active methods of noise control for industrial fans are then discussed, and a possible way of a more advanced solution for using ANC on larger axial fans is proposed.

1. Introduction

The noise of fans arises mainly aerodynamically from the rotating blades of the impeller, and usually consists of tonal sound components and broadband random noise. Tonal components occur at the blade passing frequency or also at its multiples, and come mainly from the trails in the air generated by the moving blades. The broadband noise is associated with random fluctuations in the flow on and around the blades. Both the tonal and the random noise rise rapidly with increasing rotation speed of the impeller.

Most of the random noise comes from the eddy swirls following the trailing edges of the blades and the blade tips. When a blade tip cuts through the air, it leaves a spinning trail in the air called a vortex. The swirls produce random noise with a broad frequency spectrum. Both harmonic and random noise generation is strongest at the end parts of blades, where the speed of blades is maximal. Faster splitting of the air also means higher frequency components of the noise radiated mainly by the blades tips.

In the absence of stronger upstream disturbances in the air stream, rotating blades radiate noise basically due to three following mechanisms: (1) the vortices mainly at the blade tips, (2) the vortex-shedding mostly due to trailing-edge thickness and (3) the scattering of the boundary-layer turbulences at the trailing edges of the blades. Fan noise also depends on the aerodynamic load and can be increased considerably by disturbances of the input stream of air, as e.g. caused by protective gratings.

Both the aerodynamic and acoustic properties of fans depend strongly on the shape and number of blades, or more correctly, on what is called the solidity ratio of the blades, this being the ratio of the sum of the overall blade widths to the circumference of the impeller. Blade shape and twist also affects the velocity profile of the output air stream. The shape, solidity ratio and number of blades can substantially influence spectral properties of the radiated noise, however, not as much the overall sound power of the emitted noise.

This article is mainly concerned with axial fans that have an open suction side and a duct on the output side. In general, ducts on the output side of the fan can reduce drag effects of the blade tip vortices which also reduces the noise radiated into the duct. Ducted fans can run more smoothly and create the same amount of thrust with shorter blades. More information concerning the noise generated by fans can be found in the next chapter and mainly in the references to this paper.

2. Fan noise in brief

As already mentioned, fan noise originates mainly aerodynamically from the rotating blades of the impellers. Its tonal components come from the pulses of air as the moving blades push into the air. The broadband noise is generated by random fluctuations in the flow around the blades. Most of the random noise comes from the eddy swirls following the trailing edges and mainly tips of blades.

Contemporary understanding of aerodynamically generated noise basically emerges from the research done by Lighthill, namely from his papers published in 1952 and 1954 respectively [1]. In 1969 Ffowcs Williams and Hawkings published the basic relation for the noise emitted by bodies moving in air, often called the Ffowcs Williams – Hawkings relation (FW-H) [2]. These authors also introduced the three different noise source terms: (1) thickness (monopole), (2) loading (dipole), and (3) the quadruple term. The quadruple term and the corresponding noise component are largely transonic phenomena, and can be ignored at the subsonic regime in which the industrial fans work.

The FW-H equation was derived from Lighthill's acoustic analogies under the assumption of a limited source region, which is enclosed by a specified control surface. In this way, the volume integration for monopole and dipole partial noise sources can be superseded by surface integrals. If necessary, noise sources outside the control surface can be accounted for by subsequent volume integration.

In 1998 Farassat and Brentner proposed a method to predict noise caused by rotating blades [3], based on FW-H relations. Subsequently, Farassat published the next papers leading to his formulations 1 and 1A which since then have been used mainly for computing propeller noise [4]. The Farasat formulations 1 and 1A are solutions of the

Přijato 24. dubna 2014, akceptováno 19. prosince 2014.

Ffowcs Williams-Hawkings equation with surface sources moving at subsonic speed. The last paper dealing with these formulations was published in 2007 [5].

A good overview of noise prediction methods aimed mainly at axial fans appeared in 2000 [6]. Probably the first attempts to extend the Computational Fluid Dynamics (CFD) methods and software to compute noise generated by fans were published in 2003 [7] and 2004 subsequently [8].

A number of papers dealing with fan noise were published through years 2007 to 2012 [e.g. 9–13], aimed in greater detail at the broad-band noise generated by trailing edges and at tips of the blades. Several very interesting papers appeared in 2013, dealing e.g. with the noise generated by spinning-tip and trailing-edge turbulences [14, 15, 39, 40] and, probably for the first time as well with the spinning-waves modes of the noise generated by fans in ducts [16].

Regrettably not even the latest advancements in understanding fan noise nor the contemporary advanced CFD/CAE computational means (e.g. FLUENT [17] and similar others) have brought particularly new findings to the further reduction of fan noise, nor anything that would not have been known or found experimentally. To illustrate this assertion let us take an example the two fans shown in Figs. 1 and 2.

Figure 1: Fan 1 – impeller with six broad and relatively curved blades *(high solidity ratio)*

The impellers of the two fans differ in the shape and number of blades and also by the solidity ratio of the blades on the impellers. The typical spectral characteristics of the noise of the two fans can be seen in Figs. 3 and 4. The analyzed noise samples of the two fans have been recorded at the free suction side of the fans, 60 degrees off the fans axis, at a distance of 2 m from the impeller center, and at the same rotational speed of the impellers. In Figs 3 and 4 and also in the subsequent frequency spectra, the dark and light blue curves indicate a range of short-time fluctuations.

Figure 2: Fan 2 – impeller with four narrower blades *(low solidity ratio)*

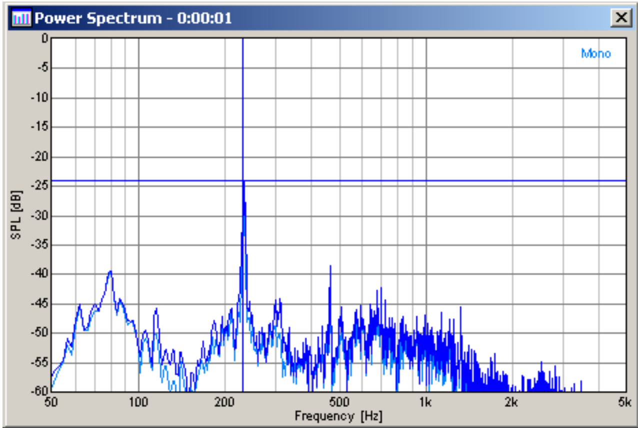

Figure 3: Frequency power spectrum of the noise sample of fan 1 (for further details see text)

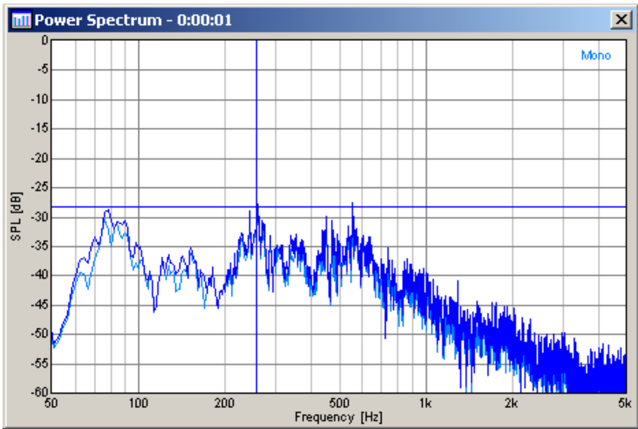

Figure 4: Frequency power spectrum of the noise sample of fan 2 *(for further details see text)*

Easily noticeable in Fig 3 is a prominent discrete spectral component at the frequency of cca 240 Hz, and the second one, weaker, at 480 Hz. With six blades, the frequency 240 Hz corresponds to 2 400 rpm of the impeller. At 480 Hz it is clearly the 2^{nd} harmonics of the blade passing frequency. The striking discrete spectral component at 240 Hz has its maximum nearly 20 dB above the mean level of the remaining noise components and about 15 dB above the maxima of the remaining part of the frequency spectrum. The second power spectrum in Fig. 4 has no visible discrete spectral component. In these figures, the light and dark blue parts of the curves merely indicate certain time fluctuations in the spectra.

In the next Figs. 5 and 6 3-D spectrograms are shown of the noise of the same two fans recorded at the same points, for their rotations changing continuously with the time from approx. 1 600 to 2 400 rpm. Clearly visible in Fig. 5 again is the tonal component at the blade passing frequency, the prominence of which increases rapidly with the rotational speed of the impeller. The increase in its level is about 15 dB whereas the rotational speed of the impeller has increased 1.5 times. Levels of the non-periodic spectral components rise much more slowly with rotations at both fans. In Fig. 6, no stronger discrete tonal component is again visible.

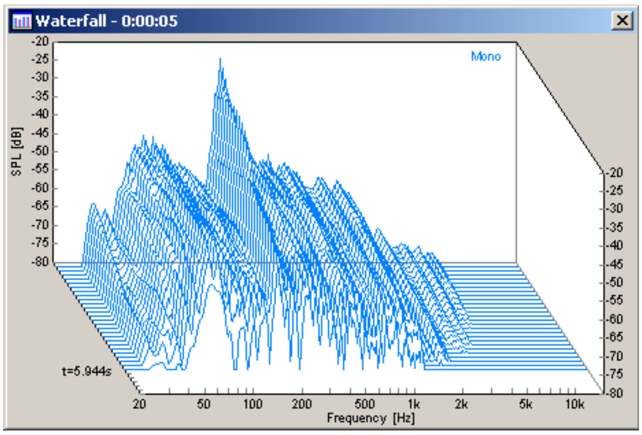

Figure 5: 3-D spectrogram – fan 1 *(time and r.p.m. go from the front backward)*

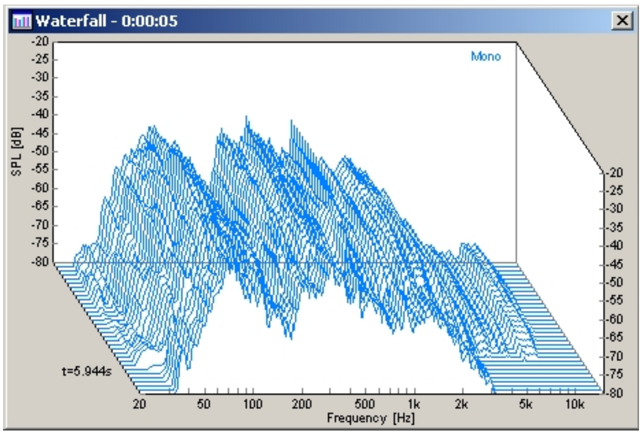

Figure 6: 3-D spectrogram – fan 2 *(time and rpm follow from the front backward)*

3. Evaluating fan noise

Noise can be assessed most simply by listening or through listening tests, or it can be based on measurements. Measured factors are mostly sound pressure levels, at a number of variously defined measuring points. A valuable tool both in noise evaluation and noise reduction is spectral analysis, and spectral decomposition, especially if the periodic and non periodic noise components are to be evaluated separately. However, the final assessment must be based on internationally accepted standards. The basic standards applicable to noise measurements of fans are listed in the following Table 1.

This paper concerns mainly axial fans with a free inlet or suction side and a duct of limited length on their output side. Under consideration is the noise radiated both from the open inlet side and the outlet of the duct. For measuring noise radiated from the free suction side, as well as from the open outlet side of the duct, the standards from the ISO 3740 “family” can be and mostly are used.

3.1. Noise radiated into free or semi-free space

In practice, the standard most often used is ISO 3744 (Determination of sound power levels and sound energy levels of noise sources using sound pressure – Engineering methods for an essentially free field over a reflecting plane), which specifies the means and conditions of determining sound power from sound pressure levels, measured on a virtual surface enveloping the noise source. The accuracy grade is 2 (engineering grade).

Most often, we measure fans with ducts. In this case, standard ISO 3744 can also be used for determining separately the sound power of the noise radiated from the suction and the outlet side of the fan assembly. This is mostly possible simply through the proper choosing or allocating of measuring points for the suction and outlet sides. An example of such measurement is shown in Fig. 7. An auxiliary adjustable cage is used for fixing the measuring points around the measured object. For measuring fans with shorter ducts, a separation wall of sufficient dimensions would, however, be necessary.

Shown in Fig. 8 is the assembly of the measured fan from the suction side. An example of the result of measurement on this fan assembly is in Fig. 9. Fb is the frequency of the power supply feeding the synchronous electromotor of the fan. The rotational speed of the impeller equals 48 × Fb [r. p. m.].

3.2. Measuring noise emitted into ducts

Measuring noise of fans emitted into ducts specifies standard ISO 5136 (Acoustics – Determination of sound power

Figure 7: Measuring noise of an axial fan with a duct according to ISO 3744

Figure 8: The measured assembly: an industrial fan with a longer duct on the output side

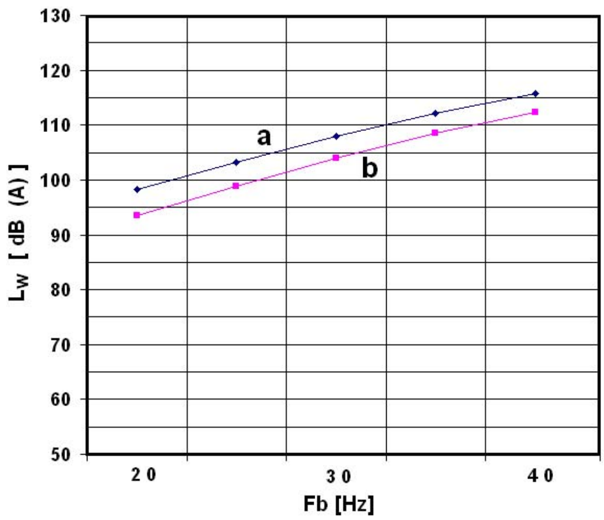

Figure 9: An example of the results of measuring the fan assembly shown in Fig.8: a – sound power from the suction side, b – sound power from the duct outlet side

Table 1: Standards used for noise measurements of fans

ISO 3740:2000 Acoustics – Determination of sound power levels of noise sources – Guidelines for the use of basic standards

ISO 3741:2010 Acoustics – Determination of sound power levels and sound energy levels of noise sources using sound pressure – Precision methods for reverberation test rooms

ISO 3742:1988 Acoustics – Determination of sound power levels of noise sources - Precision methods for discrete-frequency and narrow-band sources in reverberation rooms

ISO 3743:2010 Acoustics – Determination of sound power levels and sound energy levels of noise sources using sound pressure – Engineering methods for small movable sources in reverberant fields – Part 1: Comparison method for a hard-walled test room – Part 2: Methods for special reverberation test rooms (accuracy grade 2 – engineering grade)

ISO 3744:2010 Acoustics – Determination of sound power levels and sound energy levels of noise sources using sound pressure – Engineering methods for an essentially free field over a reflecting plane (accuracy grade 2 – engineering grade)

ISO 3745:2012 Acoustics – Determination of sound power levels and sound energy levels of noise sources using sound pressure – Precision methods for anechoic rooms and hemi-anechoic rooms

ISO 3746:2010 Acoustics – Determination of sound power levels and sound energy levels of noise sources using sound pressure – Survey method using an enveloping measurement surface over a reflecting plane (accuracy grade 3 – survey grade)

ISO 3747:2010 Acoustics – Determination of sound power levels and sound energy levels of noise sources using sound pressure – Engineering/survey methods for use in situ in a reverberant environment (accuracy grade 2/3 – engineering/survey grade)

ISO 5136:2003 Acoustics – Determination of sound power radiated into a duct by fans and other air-moving devices – In-duct method

ISO 9614:2002 Acoustics – Determination of sound power levels of noise sources using sound intensity – Part 1: Measurement at discrete points, Part 2: Measurement by scanning, Part 3: Precision method for measurement by scanning

radiated into a duct by fans and other air-moving devices – In-duct method). Defined in this standard are the ways and conditions of testing fans and other air-moving devices to determine the sound power radiated into measuring ducts terminated anechoically.

Figure 10: An example of anechoic termination on a measuring duct

Figure 11: Suction side of the measuring duct

ISO 5136 is supposed to be used with the measurement of ducts with diameters from 0.15 m to 2 m. Maximum mean flow velocity in the ducts is limited in dependence on the wind shields used on the measuring microphones. With a foam ball shield, the maximum velocity is 15 m/s; with nose cone 20 m/s; and with sampling tube 40 m/s. Requirements for the measuring facility are specified very thoroughly in this standard, with a number of variants e.g. for constructing the anechoic termination of the measuring duct.

An example of an anechoic termination of a measuring duct that we use is shown in Fig. 10. Fig. 11 shows the suction side of the same measuring duct. Shown in Fig. 12 is the disassembled suction side of the measuring duct with a fan fixed on it for subsequent measuring. The fan has 18 narrow blades.

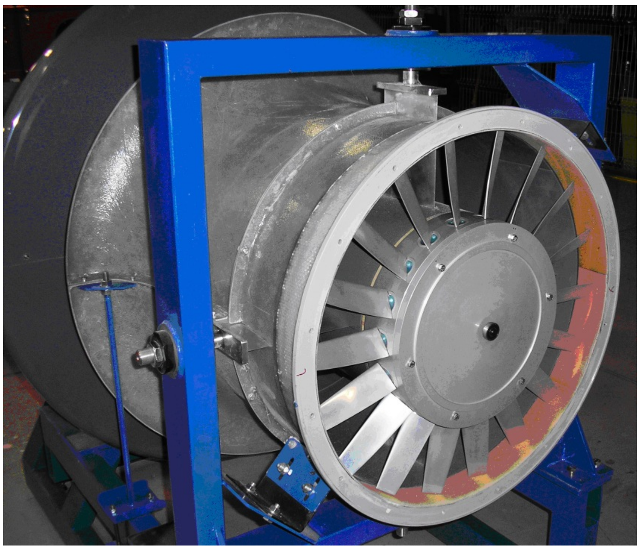

Figure 12: Measuring duct disassembled; showing a fan fixed on it

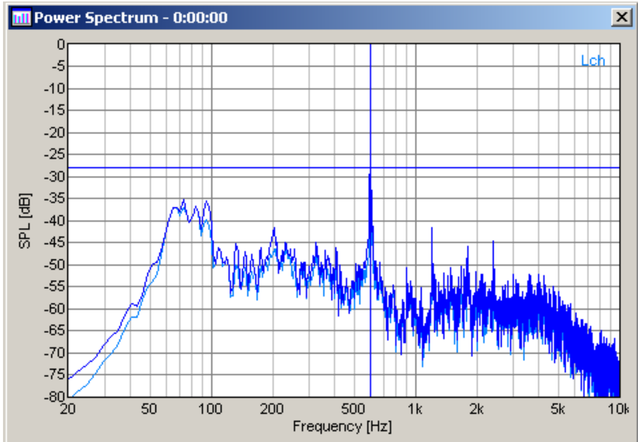

Figure 13: Frequency spectrum of the noise of the fan at 2 000 rpm *(for details see the text)*

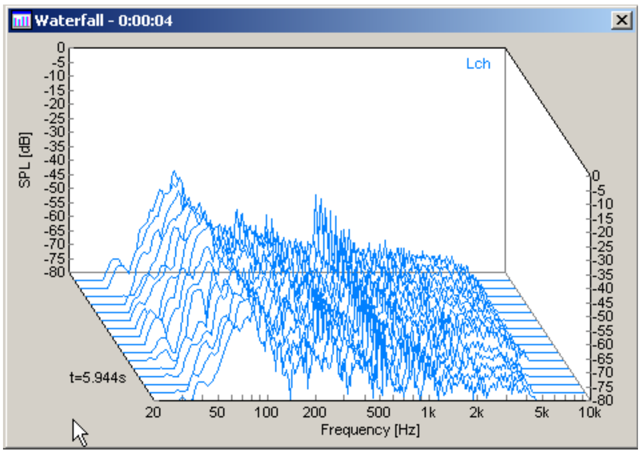

Figure 14: An example of how the spectrum of the noise can change with the microphone's radial position *(impeller rotating at 2 000 r.p.m.; time follows from the front backwards)*

An example of a frequency spectrum (spectral density distribution) typical for the fan with this impeller is shown in Fig. 13. The chosen noise sample was picked up at 2 000 rpm of the impeller by a 1/4 inch microphone with a wind screen placed inside measuring duct according to ISO 5136. The prominent spectral maximum at 600 Hz corresponds only to the first harmonics of the blade passing frequency. The light and dark blue curves in these figures merely indicate some possible time fluctuations in the spectra.

Fig. 14 shows an example of how the spectrum of the noise can change with the microphone's radial position. In this case, the microphone was moving slowly from the duct axes to the wall of the duct. The position of the microphone as prescribed by ISO 5136 can eliminate only the first circular mode. Measuring at more then one circumferential position can eliminate the first spinning mode. It should be pointed out that at higher frequencies, the uncertainty of measurements according to ISO 5136 is much higher then is mostly admitted.

4. Active noise control in fans

Active Noise Control or also Active Noise Cancellation (ANC) methods are based on the idea of reducing or cancelling an undesired noise by the same noise in the opposite phase, or more precisely by another specifically generated or controlled secondary sound coming from the ANC system. At present, these methods work well only at low sound frequencies, or if the distances between the primary and secondary sound sources are small compared to the corresponding wavelengths, which also means effectiveness only in a limited space.

There are basically two ANC strategies. The first one is called feed-forward strategy (FF) the second feed-back strategy (FB). Feed-back ANC minimizes the noise in the controlled zone around a sensing microphone. Feed-forward ANC version uses the reference signal from the noise before it reaches the controlled zone. Both ANC versions can be, and often are, combined.

In the simplest alternative of an ANC FB system, a microphone picks up the sound at a given point and a loudspeaker is supposed to radiate the same acoustic signal with opposite phase. Such simple ANC strategies are used in cheaper headphones. In more expensive headphones with ANC, combined FB and FF ANC systems are used instead. Basically, simple ANC systems can work successfully only where the controlled space is small, or where the sound field has insignificant differences in spatial distribution.

In e.g. cylindrical pipes, the first transversal standing wave mode starts at frequency $f_{01} = 0.58 \cdot c_0/D$ [Hz, m]. Thus, in a pipe with diameter $D = 0.5$ m the first transversal wave mode starts at $f_{01} = 403$ Hz. A simple ANC system can be used in this case successfully only at frequencies well below 400 Hz. In headphones, the controlled space is very small and thus even simple ANC systems can work successfully up to relatively high audio frequencies.

ANC systems for larger spaces, as in propeller aircraft or cars, have to use much more complicated ANC systems with advanced multi-input multi-output (MIMO) processors and multiple microphones or vibration pickups and multiple loudspeakers, often combined with electrodynamics or piezoelectric vibrators. Less complicated, "local" ANC systems could be used on individual seats or chairs.

Many different algorithms or processing schemes have been proposed for ANC systems so far. Basic information about ANC systems can be found e.g., in a primer [18]. More comprehensive information can be found e.g. in book [19] and a number of papers as [20–24]. Comprehensive sources of knowledge about ANC systems can also be found in several interesting theses [25, 26].

What seemed initially interesting were ANC applications or ANC extensions on headrests, or chairs, as on individual seats in smaller propeller aircraft, on chairs for operators of noisy machinery. Creating local "zones of quiet" has already been a topic of interest for many researchers [see e.g. 27–30]. Regrettably, the early visions turn not to be that easy to fulfill. However, more advanced solutions of ANC processing, based on the principles of virtual sensing or nonlinear ANC concepts, could still bring broader zones of quiet with considerable noise attenuation and sufficiently stable function. [31–33]

The main problem or difficulty of using ANC on industrial fans is mostly their large dimensions and the high acoustic power of the emitted noise. ANC systems for large industrial fans would have to deliver high acoustic power, and if solved by standard electro-acoustic means, they would also place great demands on input power or power supply. As yet, ANC systems have therefore been proposed instead for smaller fans, such as those used for cooling computers or larger electronic systems.

The noise of cooling fans in electronic systems has been receiving increasing attention in recent years as one of the competitive factors. As yet, reducing noise of small fans has been solved in passive ways, mainly by improving the aerodynamics of the impellers and by applying sound-absorbing materials. Recently, however, fairly new companies have started advertising cooling fans for electronic systems using an advanced proprietary solution of ANC technology [34, 35]. According to our measurements on one of the advertised smaller cooling fans, the effect achieved has not been found exceptional as can be documented by Figs. 15–17.

As can be seen from Figs. 15–17, again, only the tonal components of the noise are suppressed distinctly, whereas the nondeterministic noise components remain nearly intact. Regrettably, this confirms again that only a small effect of ANC can be expected so far on random noise without perceivable tonal components. *On the contrary, a considerable effect from ANC systems could be expected with fans for which their noise contains prominent tonal components.*

Fairly lower noise could be reached very probably by using ANC on smaller fans with impellers purposely designed for the lowest random noise at the cost of more prominent tonal noise components. Development of low-noise fans based on the above idea could be very likely an interesting topic for further research. Another topic aimed

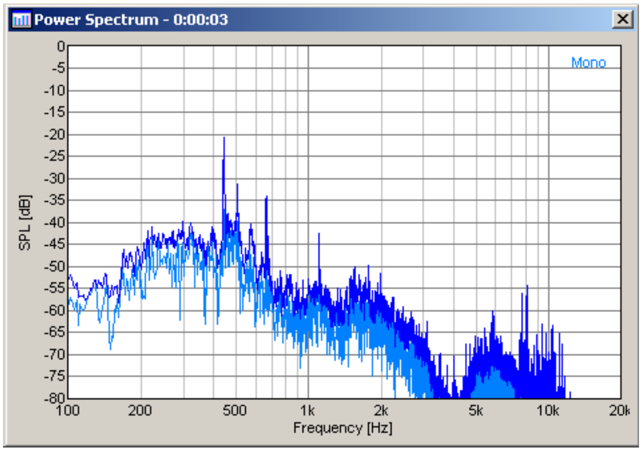

Figure 15: Frequency spectrum of the noise of an advertized cooling fan – ANC switched off

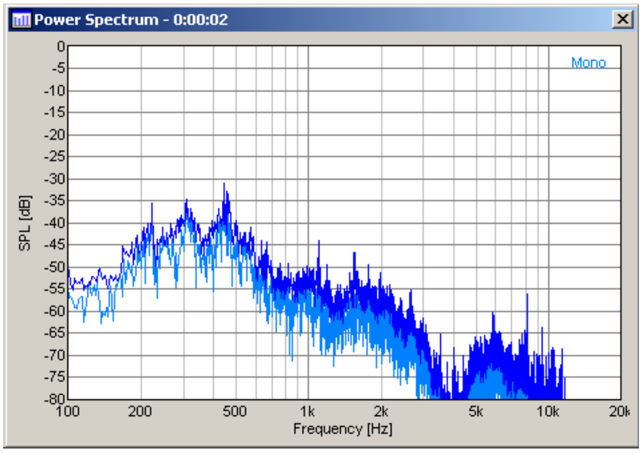

Figure 16: Frequency spectrum of noise of the same cooling fan – ANC switched on

mainly at fans with ducts could be based on the so-called modal concept [36–38].

Ensuing from these two concepts, it could be interesting to place the source of the noise-cancelling sound not on the walls of the duct, as has been the present practice, but coaxially with the impeller of the fan. A coaxial, possibly annular source of the noise-cancelling acoustic signal could very probably also solve the problem of cancelling the spinning modes of the noise excited by the rotating blades.

5. Summary and conclusions

Fan noise consists of tonal sound components and broadband random noise. Tonal components occur mostly at the blade passing frequency and its multiples. Broadband noise is generated by random fluctuations in the flow on and around the blades. Random noise arises from the eddy swirls following the trailing edges of the blades and mainly from or around the blade tips. The random and mainly

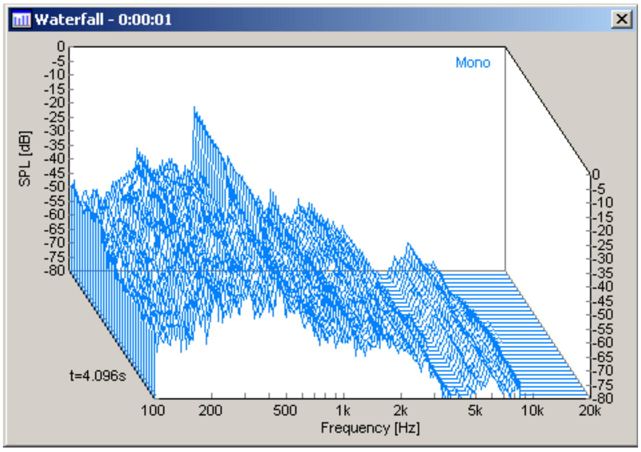

Figure 17: 3-D spectrogram of the noise of the same fan – ANC first switched on and than off. *(time runs from the front backward)*

tonal noise levels rise rapidly with the speed of rotations of the impeller.

Both the aerodynamic and noise properties of fans depend strongly on the shape and number of blades, or also on the “solidity” ratio of the blades, i.e. the ratio of the sum of the overall blades widths to the impeller circumference. The shape, the number of blades and the solidity ratio of the impeller can substantially influence spectral properties of the radiated noise, but not as much the sound power of the noise emitted by fans.

Active Noise Control or also Active Noise Cancellation (ANC) methods are based on the idea of cancellation of an undesired noise by another specifically generated or controlled secondary sound coming from the ANC system. In practice, these methods work well only at low frequencies, and/or in a limited space. ANC systems for larger spaces, as e.g. in propeller aircraft or cars, have to use more advanced ANC solutions with multi-input multi-output (MIMO) processors, more microphones or vibration pickups and loudspeakers, often with electrodynamics or piezoelectric vibrators.

The main problem with using ANC principles on industrial fans is mostly their large dimensions and the high acoustic power of the emitted noise. ANC systems for large industrial fans would have to deliver high acoustic power, and if solved by standard electro-acoustic means, would also demand considerable input power or power supply. Consequently, up to now ANC systems have been used instead on smaller fans, e.g. for cooling electronic systems.

A very small effect can be expected from known ANC systems in application to noise having weak or no tonal components. On the contrary, a considerable effect of ANC could be reached with fans having lower random noise and more prominent tonal noise components, possibly even having the impellers purposely designed towards this end. Further research would, however, be needed to verify the effect attainable in this way.

A promising way to reduce the noise of fans radiated into ducts seems to be placing the source of the noise-cancelling sound not only on the walls of the duct, as mostly found in the present concepts, but inside the duct and coaxially with the impeller. A coaxial or possibly annular source of the noise-cancelling signal near the hub of the impeller could solve also the problem of cancellation of the spinning modes of noise in ducts. Proving these ideas would, however, require further research.

References

[1] LIGHTHILL, M. J.: On the sound generated aerodynamically, Part I. General Theory, Proc. Royal Soc. (A), Vol. 211, pp. 564–87, 1952, Part II, Turbulence as a Source of Sound, Proc. Royal Soc. (A), Vol. 222, pp. 1–32, 1954

[2] FFOWCS WILLIAMS, J. E., HAWKINGS, D. L.: Sound generated by turbulences and surfaces in arbitrary motion, Philosophical Transactions of the Royal Society, Series A, Vol. 264, pp. 321–342, 1969

[3] FARASSAT, F., BRENTNER, K. S.: The acoustic analogy and the prediction of the noise of rotating blades, Theor. and Comp. Fluid Dynamics, Vol. 10, No. 1–4, 1998

[4] FARASSAT, F.: Acoustic Radiation From Rotating Blades – The Kirchhoff Method, NASA Langley Research Center, July, 2000

[5] FARASSAT, F.: Derivation of formulations1 and 1A, NASA / TM – 2007-214853, Langley Research Center, Hampton, Virginia, 2007

[6] CAROLUS, T., SCHNEIDER, M.: Review of Noise Prediction Methods for Axial Flow Fans, Inter-noise 2000, Nice, France, August 2000

[7] LYRINTZIS, A. S.: Integral acoustics methods: From the (CFD) Near-field to the (Acoustic) Far-field, Internat. Journ. of Aeroacoustics, Vol. 2, No. 2, pp. 95–128, 2003

[8] CASPER, J., FARASSAT, F.: Broadband trailing edge noise predictions in the time domain, J. Sound Vib., Vol. 271, pp. 159–176, 2004

[9] CARO, S., SANDBOGE, R. at all: CAA Formulation on Fan Noise based on Lighthill's Analogy for Fan Noise, Fan Noise 2007, Lyon (France), 17–19 September 2007

[10] ENGHARDT, L.: Improvement of Fan Broadband Noise Prediction: Experimental Investigation and Computational Modelling, Final Project Report: Proband-DLR-WP1-Task 1.0, DLR 2009

[11] ROZENBERG, Y., MOREAU, S., HENNER, M., MORRIS, S. C.: Fan trailing edge noise prediction using RANS simulations. 16th AIAA/CEAS Aeroacoustics Conf. AIAA-2010-3720, 2010

[12] TAKAAKI, H., NOBUHIKO, Y., TSUTOMU, O.: Numerical Simulation for Fan Broadband Noise Prediction, J. Thermal Science, Vol. 20, No. 1, pp. 58–63, 2011

[13] CORSINI, A., RISPOLI, F., SHEARD, A. G., TEZDUYAR, T. E.: Computational analysis of noise reduction devices in axial fans with stabilized finite element formulations, Computational Mechanics, Volume 50, Issue 6, pp. 695–705, Dec. 2012

[14] ZHU, T., CAROLUS, T. H.: Experimental And Numerical Investigation of The Tip Clearance Noise of an Axial Fan, Proc. of ASME 2013, Turbine Blade Tip Symposium TBTS 2013, Hamburg, Germany

[15] SAHILI, A., ZOGHEIB, B., BARRON, R.: 3-D Modeling of Axial Fans, Applied Mathematics, pp. 632–651, 2013

[16] WEI, Q., XUN, H., PEERS, E.: Acoustic imaging of a duct spinning mode by the use of an in-duct circular microphone array, J. Acoust. Soc. Am., Vol. 133, No. 6, June 2013

[17] Fluent Inc., FLUENT 6.1 – Acoustics Module Manual, [online], February 2003, [Accessed 10 December 2014] Available from: `http://jullio.pe.kr/fluent6.1/help/pdf/acoustics/fl61aco.pdf`

[18] KUO, S. M., MORGAN, D. R.: Active Noise Control: A Tutorial Review, Proc. of the IEEE, Vol. 87, No. 6, June, 1999

[19] NELSON, P. A., ELLIOTT, S. J.: Active control of sound, 1991, Academic press

[20] JIŘÍČEK, O., BROTHÁNEK, M.: Application of multi-channel feed-forward active control in a duct, Proc. of the Inter-noise 2001, pp. 641–644, The Hague, 2001.

[21] JIŘÍČEK, O., BROTHÁNEK, M., Application of IIR filters in multi-channel ANC in duct, Proc. of Active, 2002, pp. 773–780, Southampton, 2002

[22] SCHULZ, J., NEISE, W., MÖSER, M.: Active Noise Control in Axial Turbomachines by Low Induced Secondary Sources, 8th AIAA/CEAS Aeroacoustics Conf., Breckenridge, Colorado, USA, June, 17–19, 2002

[23] NEUHAUS, L., SCHULZ, J., NEISE, W., MÖSER, M.: Active Control of Aerodynamic Performance and tonal Noise of axial Turbomachines,

5th European Conference on Turbomachinery, Fluid Dynamics and Thermodynamics, Paper No. 195, Prague, 2003

[24] SOMMERFELDT, S. D., GEE, K. L.: Active control of axial and centrifugal fan noise, J. Acoust. Soc. Am. Volume 133, Issue 5, p. 3264, 2013

[25] FRAANJE, R. : Robust and fast schemes in broadband active noise and vibration control Ph.D. Thesis University of Twentee, The Netherlands, 2004, ISBN 90-9018002-8

[26] HOMMA, K.: Compact Integrated Active-Passive Approach for Axial Fan Noise Control, Dissertation, Faculty of the Virginia Polytechnic Institute and State University 2004, Available from: `http://scholar.lib.vt.edu/theses/available/etd-09232004-204237/unrestricted/etd_kenji_homma.pdf`

[27] BROTHANEK, M, JIRICEK, O.: Formatting zones of quiet around a head simulator, Proc. Active-2002, Southampton, UK, pp. 117–121, 2002

[28] JIŘÍČEK, O., BROTHÁNEK, M.: Experiments with Local Active Noise Control in Passenger Seats, Proc. of Euronoise 2003, ISBN 88-88942-00-9

[29] JIŘÍČEK, O., BROTHÁNEK, M.: Comparison of Two Secondary Sources Configurations for Active Headrest, Proc. of Inter-noise 2003, 436–443, Jeju, Korea, 2003

[30] PAWELCZYK, M.: Adaptive noise control algorithms for active headrest system, Control Engineering Practice Volume 12, Issue 9, Sept. 2004

[31] MOREAU, D. (at all): Review of Virtual Sensing Algorithms for Active Noise Control, Algorithms 2008, 1, 69–99

[32] DEBI, P., MOREAU, D., CAZZOLATO, S.: Performance evaluation of an active headrest using the remote microphone technique, Paper No. 69, Proc. of ACOUSTICS 2011, 2–4 November 2011, Gold Coast, Australia, Acoustics 2011

[33] DEBI P., MOREAU D., CAZZOLATO S.: Nonlinear active noise control for headrest using virtual microphone control, Control Engineering Practice, Volume 21, Issue 4, pp. 544–555, 2013

[34] RotoSub AB: [online], [Accessed 10 December 2014] Available from: `http://www.rotosub.com/s_technology.php`

[35] Noctua ANC: [online], [Accessed 10 December 2014] Available from: `http://www.noctua.at/main.php?show=rotosub_anc_project`

[36] BENNETT, J. G., TAPKEN U. at all: Modelling Multi-Modal Sound Transission From Point Sources in Ducts with Flow Using a Wave-based Method, ICVS 16, Krakow, 5–9 July 2009

[37] TAPKEN, U., YANCHANG ZHANG, Y., ENGHARDT, L., NEISE, W.: A Modal Concept for Active Noise Control in Circular or Annular Ducts, RTO AVT Symposium on "Active Control Technology...", Braunschweig, Germany, 8–11 May 2000 Also available from: `http://ftp.rta.nato.int/public/PubFullText/RTO/MP/RTO-MP-051/MP-051-PSF-19.pdf`

[38] LAITA, G.: Active Noise Control: a case study, Master Graduation Thesis, Politetecnico di Milano, Academic Year 2011/2012

[39] CLAIR V., POLACSEK, C. at all.: Experimental and Numerical Investigation of Turbulence-Airfoil Noise Reduction Using Wavy Edges, AIAA Journ., Vol. 51(11): pp. 2695–2713. 11, 2013

[40] SINAYOKO, S., KINGAN, M., AGARWAL, A.: Trailing edge noise theory for rotating blades in uniform flow, Proc. Roy. Soc. A. 1–28; June 11, 2013 Also available from: `http://arxiv.org/pdf/1304.8072.pdf`

Roughness Prediction for Complex Acoustic Stimuli

Predikce vjemu drsnosti komplexních akustických signálů

Václav Vencovský[a,b]

[a]Musical Acoustics Research Center, Academy of Performing Arts in Prague,
Malostranské nám. 12, 118 00 Praha 1, Czech Republic
[b]Department of Radioelectronics, Czech Technical University in Prague,
Technická 2, 160 00 Praha 6, Czech Republic
vaclav.vencovsky@gmail.com

Vencovský [12] introduced a new roughness model and showed its performance in comparison with listening tests for three types of complex acoustics stimuli: amplitude-modulated harmonic complex tones, real samples of pathological voices (sustained vowel /a/), harmonic intervals of the chromatic scale composed of two harmonic complex tones (dyads). This study extends his results. It adds a new type of stimuli (low-frequency harmonic complex tones), slightly changes the method used to estimate roughness, and, for a comparison, depicts results for Daniel and Weber's roughness model [9], and Leman's synchronization index (SI) roughness model [10]. Vencovský's model performed well for all of the stimuli. Daniel and Weber's model performed well for the first type of stimuli, but its results were poor for the rest of the stimuli. The SI model performed well for the first three types of the stimuli but poorly for the low-frequency harmonic complex tones.

1. Introduction

Two pure tones added together create a signal with a fluctuating envelope. The frequency of the fluctuations equals the frequency difference between the tones. We may perceive the fluctuations as periodic changes of the signal loudness when the frequency of the fluctuations is below 30 Hz. When the frequency of the fluctuations slowly increases above 30 Hz, we may perceive a jarring and rough sound sensation described by the term roughness [1]. As the frequency increases, the sensation reaches its maximum and then starts to decrease. We then perceive both tones separately with pitches given by their frequency. This suggests that we perceive the roughness because the ear cannot resolve the spectral components of the sound which are close in frequency [1, 2].

Researchers have employed various psychophysical methods to measure roughness [3–7] and given roughness a unit called asper [6]. Hand in hand with the psychophysical methods, researchers developed various mathematical models predicting roughness (see [2, 6, 8–10]) but none of them have been standardized [11]. One group of the models, known as *curve-mapping* models, detects spectral components of the sound stimuli and maps them into a psychoacoustical curve of roughness [2]. However, the *curve-mapping* models cannot process signals with continuous spectra, for example, noises [10]. The second group of roughness models employs algorithms simulating the function of the peripheral ear [10]. Daniel and Weber's model [9], and Leman's synchronization index (SI) model [10] belong to this group.

The aim of this study is to extend the results of the study of Vencovský [12] which introduced a new roughness model. The model employs an algorithm simulating the function of the peripheral ear and thus belongs to the same group as Daniel and Weber's and the SI roughness models. Vencovský [12] used the model to predict results of listening tests for: amplitude-modulated harmonic complex tones, real pathological voice samples, and harmonic intervals of the chromatic scale. I slightly changed the method used to estimate roughness, verified the roughness model by a new type of stimuli (low-frequency harmonic complex tones), and, for a comparison, depicted predictions given by Daniel and Weber's, and the SI roughness model. Some of the used real pathological voice samples were rough and breathy. Speech synthesizers simulate breathiness by adding noise to the signal [13]. Since the *curve-mapping* roughness models cannot predict roughness for noise stimuli, I did not use any model of this group [10].

2. Roughness models

This section basically describes three different roughness models: Vencovský's model [12], Daniel and Weber's model [9] and synchronization index (SI) model [10].

2.1. Vencovský's model

Vencovský presented the model in the study [12]. The model has a cascade architecture consisting of two stages: a peripheral stage simulating the function of the human auditory system, and a central stage predicting roughness from the simulated neural signal at the output of the peripheral stage.

The peripheral stage – a computational auditory model – transforms an input acoustic stimulus into the simulated neural signal in auditory nerve fibers. It is composed of: an outer and middle ear model, a model of the basilar

Přijato 24. října 2014, akceptováno 11. prosince 2014.

membrane (BM) response and cochlear hydrodynamics developed by Mammano and Nobili [14–16], and algorithms simulating the function of the inner hair cells [17–20]. The signal at the output of the peripheral stage represents the simulated neural signal. Since the peripheral ear conducts spatial-frequency analyses, the output signal has 300 channels: each represents response of the peripheral ear tuned to a certain frequency between 16 Hz and 17 kHz.

The central stage calculates roughness from the simulated neural signal obtained at the output of the peripheral stage. It first extracts the signal envelope and then process it by a 1st-order Butterworth low pass filter with a cut-off frequency of 80 Hz. The filter ensures that the roughness decreases for fluctuations of higher frequencies. The central stage then extracts two features from the parts of the envelope where the signal is rising (rising slopes): duration of the rising slope, and difference between the minimal and maximal value. Roughness is estimated as a product of the frequency calculated from the duration of the rising slopes and the modulation depth calculated from the minimal and maximal value of the rising slopes [12]. This statistics takes into account the shape of the time domain envelope of the simulated neural signal and the roughness model thus predicts roughness for the stimuli not covered by Daniel and Weber's and the SI roughness model [12].

Vencovský [12, 21] designed two versions of the roughness model with a slightly different central stage. The model version described in the study [21] predicts roughness in dependence on parameters of various synthetic stimuli, for example, on the modulation frequency for amplitude-modulated tones. The study [12] presents a model which is more suitable for predicting roughness of various types of complex stimuli. This letter version of the roughness model is used in this study.

2.2. Daniel and Weber's model

Daniel and Weber [9] improved a model designed by Aures [8]. The peripheral part of the model transforms the input stimulus into a spectrum and divides it into bands of a bandwidth equal to the critical bandwidth in Barks [6]. It then turns the spectral representation of the signal in each band to the time domain and estimates the modulation depth of the signal envelope. The model employs a bank of weighting filters and was tuned to account for roughness of amplitude-modulated tones experimentally measured by Aures [22] and presented in the book of Fastl and Zwicker [6]. The model is calibrated to aspers. Daniel and Weber showed that the model accounts for roughness of various types of synthetic stimuli, for example, amplitude and frequency modulated tones, and unmodulated bandpass noises [9]. Wang *et al.* [11] used the model to predict roughness of vehicle noise.

2.3. Synchronization index model

Leman [10] designed the synchronization index (SI) model. The model employs an auditory model which transforms the input acoustic stimulus into bands of the bandwidth equal to the critical bandwidth. The signal in each band represents the simulated neural signal in auditory nerve fibers. The simulated neural signal is then filtered by bandpass filters in order to predict the bandpass characteristics of roughness when it is depicted as a function of the modulation frequency [6]. The model calculates a degree of phase locking of the filtered simulated neural signal to a particular frequency as a ratio between the short-term spectra of the simulated neural signal and the DC component of the simulated neural signal summed across all bands. Leman [10] depicted the model predictions for amplitude-modulated tones and for harmonic intervals of the chromatic scale but did not compare the results with subjective data. Wang [23] used this model to predict roughness of vehicle noise.

3. Experiment 1: Roughness of amplitude modulated harmonic complexes

Experiment 1 estimates the roughness of amplitude-modulated (AM) complex tones. I conducted a rating listening test to measure the roughness of the stimuli and compared the subjective results with predictions of the roughness models.

3.1. Method

Stimuli Harmonic complexes composed of the first three harmonics at frequencies of 300, 600 and 900 Hz were used as stimuli. All three harmonics were amplitude-modulated by the same sinusoidal signal with a frequency of 30, 40, 50, 60, and 70 Hz. Modulation depth – calculated as $20\log_{10} m$, where m is the modulation index ranging from 0 to 1 – was 0, −3, −6, −9 and −12 dB. Amplitude of the first, second and third spectral component was 0, −10 and −20 dB, respectively. Duration of the stimuli was 600 ms and they were ramped on and off with 30 ms raised-cosine ramps. The level of the stimuli was 75 dB SPL. Combination of the modulation frequencies and the modulation depths led to 25 different stimuli.

Listeners: Five experienced listeners - one woman, four men, age ranging between 25 and 44 years, including the author of this study - participated in the experiment. The listeners had normal hearing; pure-tone thresholds below 20 dB HL for frequencies between 250 Hz and 8 kHz.

Procedure and equipment: Roughness of the stimuli was rated on a discrete scale from 1 to 7 in steps of 1, where 1 was for the lowest and 7 for the highest roughness. This procedure was inspired by the study of Patel *et al.* [7] which estimated the roughness of pathological voice

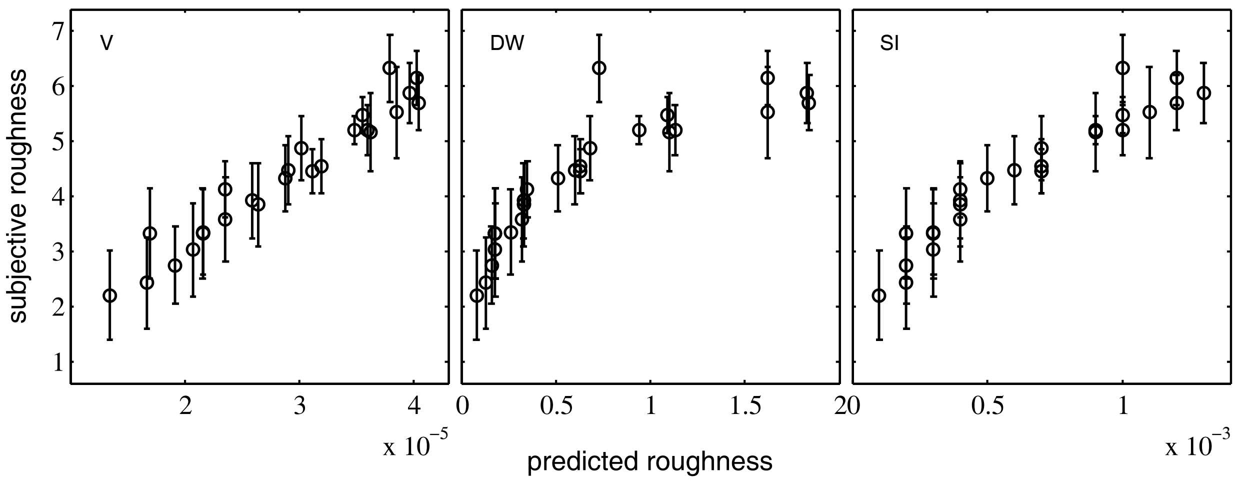

Figure 1: Mean values of the subjective ratings of roughness for amplitude-modulated harmonic complex tones plotted as a function of the roughness predicted by Vencovský's model (left panel), Daniel and Weber's model (center panel), and the SI model (right panel).

stimuli on a 5 point scale. Just noticeable difference of roughness corresponds to about 10% change of the modulation index, m, of a sinusoidally amplitude-modulated tone [6]. The five chosen values of the modulation depths (0, −3, −6, −9 and −12 dB) of the AM complexes should thus cause perceptible changes of roughness. Moreover, the roughness of the stimuli depends as well on the modulation frequency [6]. Thus for the AM complex stimuli, a 5 point scale seemed to be too course. The listeners rated the roughness of 25 different stimuli presented in a random order. Each stimulus was rated separately. The listeners could listen to it as many times as they desired and after assigning the roughness rating, they were presented with the next stimulus. The listening test was composed of 10 sets of randomly ordered 25 stimuli. In other words, each stimulus was rated 10 times giving the overall number of 250 stimuli in the test. The test was conducted on a computer. The stimuli were presented diotically (the same signal to both ears) via Sennheisser HD-600 headphones.

Roughness prediction: The roughness of the AM complexes was predicted by means of three types of roughness models: Vencovský's model [12], Daniel and Weber's model [9] implemented in the sound analyses software PsySound3 [24], and the synchronization index (SI) model [10] implemented in IPEM toolbox [25]. All types of models predict roughness in the time domain and give time-dependent values of roughness. Daniel and Weber's model implemented in PsySound3 and the SI model implemented in IPEM toolbox calculates the resulting value of the predicted roughness as median of the time-dependent values. Since both models calculate medians, this method is in this study also used for Vencovský's roughness model. It differs from the previous study of Vencovský [12] where the maximum of the time-dependent values of roughness was taken. This change did not have any strong effect on the predicted roughness in comparison to the previous study [12].

3.2. Results

Each stimulus was rated ten times, but the first two ratings were not taken into account for the final processing of the results. Cronbach's alpha calculated from the ratings given by each listener was in all cases higher than 0.8 with 5% level of significance, which means that the listeners were reliable. I estimated as well the intersubject reliability between mean ratings for each stimulus. Cronbach's alpha was 0.951 with 5% level of significance.

Fig. 1 shows mean values and standard deviations from the mean calculated across all listeners and ratings plotted as a function of roughness predicted by Vencovský's model [12] (left panel), Daniel and Weber's model [9] (center panel), and the SI model [10] (right panel). Daniel and Weber's model predicts roughness in aspers. The presented roughness model and the SI model predicts roughness in its own model units. Tab. 1 shows Spearman's (s.c.) and Pearson's (p.c.) correlation. All three types of roughness models gave data which correlate with the subjective ratings.

Table 1: Correlation between model predictions and subjective data for amplitude-modulated harmonic complex tones.

		V	DW	SI
Spearman	r:	0.971	0.961	0.977
cor.	p:	$7 \cdot 10^{-16}$	$2.3 \cdot 10^{-14}$	$6.2 \cdot 10^{-18}$
Pearson	r:	0.973	0.863	0.956
cor.	p:	$4.7 \cdot 10^{-16}$	$2.8 \cdot 10^{-14}$	$9.4 \cdot 10^{-14}$

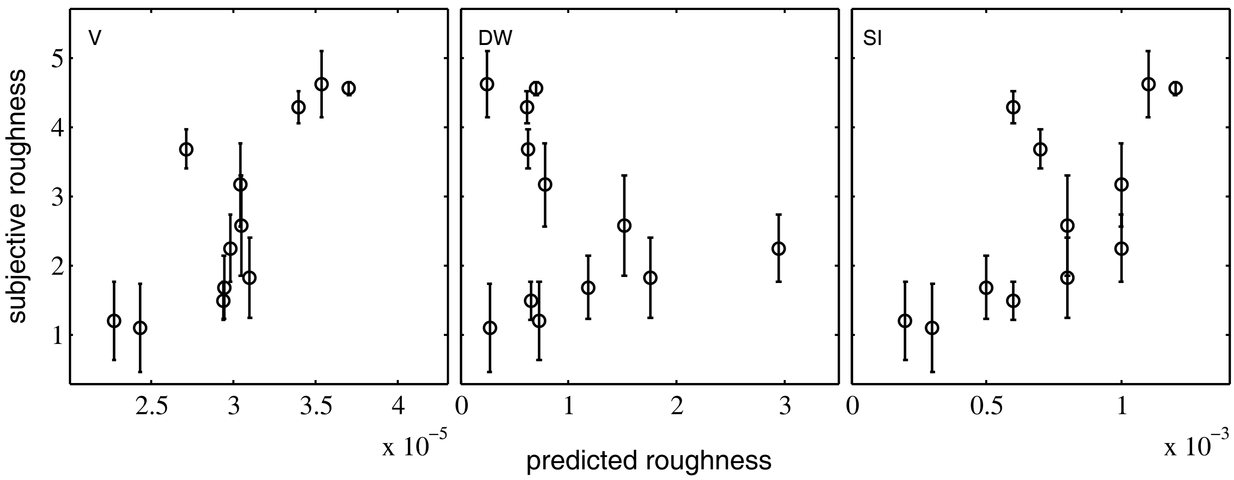

Figure 2: Mean values of the subjective roughness ratings for real voice samples – sustained vowels /a/ – plotted as a function of the roughness predicted by Vencovský's model (left panel), Daniel and Weber's model (center panel), and the SI model (right panel).

4. Experiment 2: Roughness of real voice samples

I have used the same approach as in Experiment 1 to estimate the roughness of real pathological voice samples – sustained vowels /a/.

4.1. Method

Stimuli: The stimuli were 12 real pathological voice samples of a sustained vowel /a/. The samples were extracted from stimuli recorded from 11 different subjects during the scale singing. The subjects had a pathology affecting their larynx. The stimuli differed in the pitch and in the amount of roughness. Duration of the stimuli was 300 ms and they were ramped on and off by 30 ms raised-cosine ramps. The level of the stimuli was 75 dB SPL.

Listeners: Six experienced listeners – men aged between 25 and 36 years, including the author of the study – participated in the experiment. The listeners had normal hearing; pure-tone thresholds below 20 dB hearing level (HL) for frequencies between 250 Hz and 8 kHz.

Procedure and equipment: Roughness was rated on a discrete 5-point scale from 1 to 5 in steps of 1, where 1 was for the lowest and 5 for the highest roughness. The same scale was used in the study of Patel *et al.* [7] estimating roughness of the same type of stimuli – pathological voice samples of a sustained vowel /a/. The procedure and equipment were the same as in Experiment 1. Randomly ordered 12 stimuli were rated 10 times, giving 120 stimuli.

Roughness prediction: Methods used to predict roughness were the same as in Experiment 1.

4.2. Results

As in Experiment 1, each stimulus was rated ten times, but the first two ratings were not taken into account for the final processing of the results. Intrasubject reliability estimated as Cronbach's alpha was for all listeners higher than 0.9 with 5% level of significance. Intersubject reliability estimated as Cronbach's alpha was 0.983 with 5% level of significance. I calculated the final subjective ratings as mean values across all ratings and listeners.

Fig. 2 shows the mean values and standard deviations from the mean of the subjective ratings plotted as a function of roughness predicted by Vencovský's model (left panel), Daniel and Weber's model [9] (center panel), and the SI model [10] (right panel). Daniel and Weber's model predicts roughness in aspers. The presented roughness model and the SI model has its own model units. Tab. 2 shows Spearman's (s.c.) and Pearson's (p.c.) correlation between the subjective and predicted roughness. Daniel and Weber's model predictions do not correlate with the subjective ratings. Vencovský's roughness model predicted roughness data which correlate with subjective results, but the model's performance is poor in the middle of the roughness scale. The results for the SI model are also poor in the middle of the roughness scale.

Table 2: Correlation between the model predictions and subjective data for real pathological voice samples – vowel /a/.

		V	DW	SI
Spearman	r:	0.790	−0.077	0.727
cor.	p:	$3.6 \cdot 10^{-3}$	0.817	$4.9 \cdot 10^{-3}$
Pearson	r:	0.790	0.114	0.680
cor.	p:	$2.3 \cdot 10^{-3}$	0.725	0.011

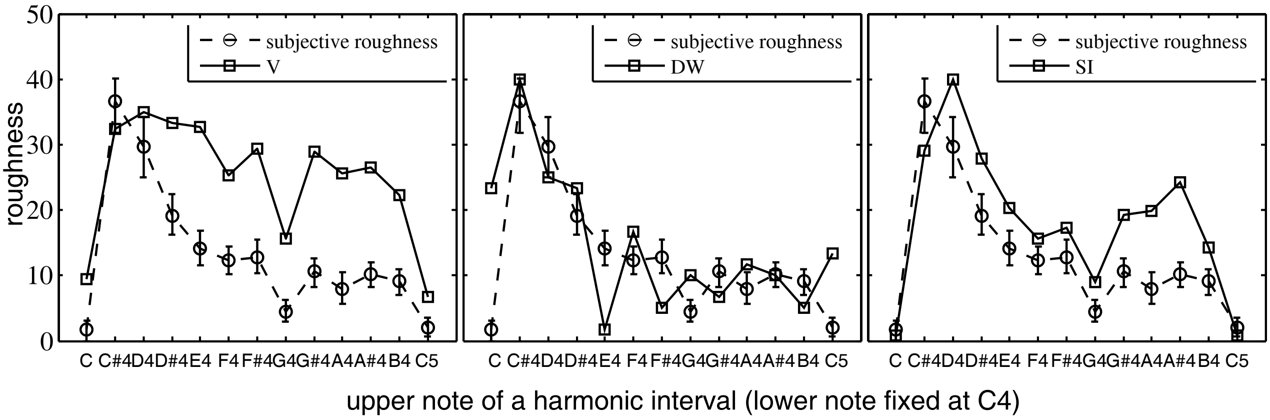

Figure 3: Roughness ratings for the harmonic intervals constructed from synthetic complex tones. Circles connected by dashed lines represent mean values of the subjective data across ten listeners reproduced from the study [2]. Squares are the roughness model ratings for Vencovský's model (left panel), Daniel and Weber's model (center panel), and the SI model (right panel).

5. Experiment 3: Roughness of intervals of the chromatic scale

In Experiment 3, I compared the subjective roughness ratings of harmonic intervals of the chromatic scale with model predictions. I reproduced the subjective ratings of roughness from the study of Vassilakis [2].

5.1. Method

Stimuli: The stimuli were constructed according to the description given in the study of Vassilakis [2]. The harmonic intervals were composed of dyads of harmonic complex tones. The complexes were composed of the first six harmonics with amplitude A_n of the nth harmonic given by the equation $A_n = A_1/n$, where n is the number of the harmonics. The fundamental frequency of the lower harmonic complex tone in the dyad was set to middle C (C4, fundamental frequency 256 Hz, equal temperament). The duration of the stimuli was 1 second and it was ramped on and off by 30 ms raised cosine ramps. The level of the stimuli was 75 dB SPL.

Listeners and procedure: Vassilakis [2] conducted the listening test with ten experienced listeners. They rated roughness on a continuous scale between 0 (not rough) and 42 (rough). The stimuli were presented diotically (the same signal to both ears) via earphones. The listeners' task was to set the position of a scroll according to the perceived roughness.

Roughness prediction: The methods used to predict roughness were the same as in Experiment 1.

5.2. Results

Squares connected by dashed lines in all panels of Fig. 3 show the subjective ratings of roughness of harmonic intervals of the chromatic scale reproduced from the study of Vassilakis [2]. The data are plotted as a function of the frequency of the higher tone in dyads. Circles connected by solid lines represent roughness predicted by Vencovský's model (left panel), Daniel and Weber's model [9] (center panel) and the SI model [10] (right panel). The model predictions were divided by its corresponding maximal values and multiplied by 40 to be in the range between 0 and 40. Tab. 3 shows Spearman's (s.c.) and Pearson's (p.c.) correlation between the subjective and predicted data. The presented roughness model successfully predicts the lowest roughness for the intervals of octave and also reflects the dip for the interval G4. The predicted roughness fits mainly the rank order of the subjective roughness as is reflected by the high Spearman's correlation and lower Pearson's correlation. The data were also well predicted by the SI model. Daniel and Weber's model predictions did not fit the subjective data well.

6. Experiment 4: Low-frequency harmonic complex tones

Miśkiewicz and Majer [26] estimated the perceived roughness of low-frequency harmonic complex tones. The results of their behavioral study are compared with predictions of the roughness models.

Table 3: Correlation between the model predictions and subjective data for harmonic intervals of the chromatic scale.

		V	DW	SI
Spearman	r:	0.918	0.224	0.852
cor.	p:	0	0.46	$3.4 \cdot 10^{-5}$
Pearson	r:	0.764	0.649	0.846
cor.	p:	$2.4 \cdot 10^{-3}$	0.016	$2.7 \cdot 10^{-4}$

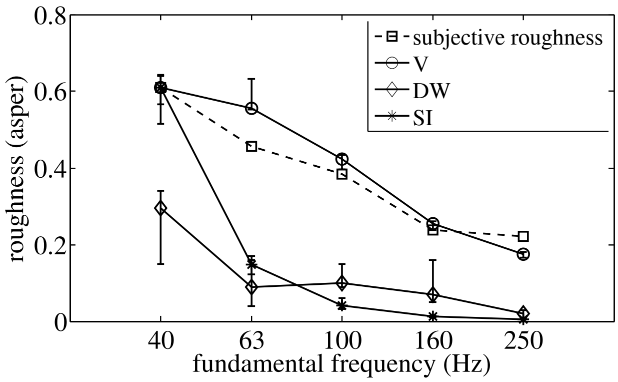

Figure 4: Roughness ratings for low-frequency harmonic complexes. The abscissa denotes a fundamental frequency of the complexes. The ordinate denotes roughness in aspers. Squares connected by dashed lines represent geometric mean values of the subjective data reproduced from the study [26]. Circles, diamonds, and asterisks represent medians and quartiles of the roughness predicted by Vencovský's model, Daniel and Weber's model and the SI model, respectively. Daniel and Weber's model predicts roughness in aspers. The presented roughness model and the SI model data were normalized by its maximal value and multiplied by the maximal subjective roughness.

6.1. Method

Stimuli The stimuli were harmonic complex tones composed of nine harmonics. The fundamental frequency of the harmonics was 40, 63, 100, 160 and 250 Hz. The spectral components were added in random phase. Amplitudes of the harmonics decreased with 6 dB per octave. Loudness of the stimuli was set to 60 phons. It was set by a loudness model designed by Moore *et al.* [27] and implemented in the sound analyses software PsySound3 [24]. Miśkiewicz and Majer [26] used 2.5-second-long stimuli ramped on and off with 2 ms cosine-squared ramps. The duration of the stimuli presented to the roughness models was 1 second. The shorter stimuli did not affected the predicted roughness but decreased computational time.

Listeners and procedure Miśkiewicz and Majer [26] obtained the behavioral data with a group of 10 experienced listeners. They used the method of absolute magnitude estimation, where listeners assign a number according to perceived roughness.

Roughness prediction: The methods used to predict roughness were the same as in Experiment 1.

6.2. Results

Fig. 4 shows the subjective and predicted roughness of low-frequency harmonic complex tones. Squares connected by dashed lines represent geometric means from 50 roughness estimates (10 listeners x 5 estimates) reproduced from the study of Miśkiewicz and Majer [26]. Circles, diamonds, and asterisks represent medians and quartiles of roughness predicted by Vencovský's model, Daniel and Weber's model [9] and the SI model [10], respectively. Since the complex tones were generated with random starting phases of the individual harmonics, the roughness was predicted for ten different harmonic complex tones with the same fundamental frequency. Daniel and Weber's model predicts roughness in aspers, while Vencovsk'y's model and the SI model are not. I normalized the predicted data given by these two roughness models by its corresponding maximal value and multiplied them by the maximal value across the subjective data.

Vencovský's roughness model qualitatively predicted the subjective data for the low-frequency harmonic complex tones. Beside the roughness of the low-frequency harmonic complex tones, Miśkiewicz and Majer [26] showed that low-frequency unmodulated pure tones may also contain roughness. The presented roughness model cannot account for this observation because it predicts roughness from the envelope of the simulated neural signal is without any modulations for unmodulated pure tones. This maybe the reason why the roughness model predicted roughness of the 40 Hz complex tone as almost equal to the roughness of the 63 Hz complex tone. Daniel and Weber's model underestimated roughness of the low-frequency complexes, and the SI model overestimated roughness of the 40 Hz complex tone. The SI model predicts roughness from the energy at low-frequencies which probably caused this overestimation.

I did not calculate Spearman's and Pearson's correlation between the subjective and predicted data because there were only four different stimuli and the agreement between the data is evident from the depicted results in Fig. 4.

7. Conclusion

The aim of this study was to extend the study of Vencovský [12] which introduced a new roughness model and compared its performance with results of listening tests. The study used three types of stimuli: amplitude-modulated harmonic complex tones, real pathological voice samples, and harmonic intervals of the chromatic scale. This study slightly changed the method used to estimate roughness for Vencovský's model. The model processes the input signal in short time frames and gives time-dependent value of the predicted roughness. The study [12] estimated the overall roughness as a maximal value across the time frames, this study calculates median across the time frames. Beside this, I added a new type of stimuli (low-frequency harmonic complex tones), and depicted results for two other roughness models: Daniel and Weber's model [9] and the synchronization index (SI) model [10].

Spearman's and Pearson's correlation described the fit between the predicted and subjective roughness of the used stimuli. Results obtained by Vencovský's roughness model correlated with the subjective data for all of the tested stimuli; Spearman's correlation higher than 0.764, and Pearson's correlation higher than 0.790. The model also predicted the subjective roughness of low-frequency harmonic complex tones (Experiment 4). Daniel and Weber's model performed well only for the first type of stimuli (Experiment 1, amplitude-modulated harmonic complex tones), and gave the worst predictions for the real pathological voice samples (Experiment 2). The SI model performed well for the first three stimuli (Experiment 1 to 3) but could not predict the subjective data for Experiment 4.

Vencovský's model performed best in comparison with Daniel and Weber's, and the SI model. It may indicate that the peripheral stage of Vencovský's model adequately simulates the physiology of the peripheral ear, and that the central stage selects features from the simulated neural signal which cover the perception of roughness. However, the model results for the real pathological voice samples (Experiment 2) were poor especially for the stimuli in the middle of the roughness scale. This should be studied further.

Acknowledgments

I would like to thank to Aleš Vetešník for sending the MATLAB scripts of the cochlear model and to Jaroslav Bouše for giving me comments on the text of the study. The research was supported by the Ministry of Education, Youth and Sports of the Czech Republic in the Long Term Conceptual Development of Research Institutes grant of the Academy of Performing Arts in Prague: The "Sound quality" project.

References

[1] von Helmholtz, H. L. F.: *On the Sensations of Tone as the Physiological Basis for the Theory of Music*, translated by A. J. Ellis (1885), 4th ed., Dover, New York, 1954.

[2] Vassilakis, P. N.: Auditory roughness as a means of musical expression, *Selected Reports in Ethnomusicology*, 12, Perspectives in Systematic Musicology, p. 119–144, 2005.

[3] Mathes, R. C., Miller, R. L.: Phase Effects in Monaural Perception, *J. Acoust. Soc. Am.* 19(**5**), p. 780–797, 1947.

[4] Terhardt, E.: On the perception of periodic sound fluctuations (Roughness), *Acustica* 30(**4**), p. 201–213, 1974.

[5] Pressnitzer, D., McAdams, S.: Two phase effects in roughness perception, *J. Acoust. Soc. Am.* 105(**5**), p. 2773–2782, 1999.

[6] Fastl, H., Zwicker, E.: *Psychoacoustics: Facts and Models*, Springer, Berlin, Heidelberg, New York, 2007.

[7] Patel, S. A., Shrivastav, R., Eddins D. A.: Identifying a Comparison for Matching Rough Voice Quality, *J. Speech Lang. Hear. Res.*, 55, p. 1407–1422, 2012.

[8] Aures, W.: Ein Berechnungsverfahren der Rauhigkeit, *Acustica*, 58(**5**), p. 268–281, 1985.

[9] Daniel, P., Weber, R.: Psychoacoustical roughness: Implementation of an optimized model, *Acustica* 83(**1**), p. 113–123, 1997.

[10] Leman, M.: Visualization and calculation of the roughness of acoustical musical signals using the synchronization index model (SIM), *Proceedings of the COST G-6 Conference on Digital Audio Effects (D AFX-00)*, Verona, Italy, DAFX 1-DAFX 6, 2000.

[11] Wang, Y. S., Shen, G. Q., Guo, H., Tang, X. L., Hamade, T.: Roughness modelling based on human auditory perception for sound quality evaluation of vehicle interior noise, *J. Sound and Vibration*, 332, p. 3893–3904, 2013.

[12] Vencovský, V..: Modeling roughness perception for complex stimuli using a model of cochlear hydrodynamics, *ISMA 2014*, Le Mans, France, 2014.

[13] Klatt, D.H.: Software for a cascade/parallel formant synthesizer, *J. Acoust. Soc. Am.* 67(**3**), p. 971–995, 1980.

[14] Mammano, F., Nobili, R.: Biophysics of the cochlea: Linear approximation, *J. Acoust. Soc. Am.* 93(**6**), p. 3320–3332, 1993.

[15] Nobili, R., Mammano, F.: Biophysics of the cochlea II: Stationary nonlinear phenomenology, *J. Acoust. Soc. Am.*, 99(**4**), p. 2244–2255, 1996.

[16] Nobili, R., Vetešník, V., Turicchia, L. Mammano, F.: Otoacoustic emissions from residual oscillations of the cochlear basilar membrane in a human ear model, *J. Assoc. Res. Otolaryngol*, 4, p. 478–494, 2003.

[17] Shamma, S. A, Chadwick, R. S., Wilbur, W. J., Morrish, K. A., Rinzel, J.: A biophysical model of cochlear processing: Intensity dependence of pure tone responses, *J. Acoust. Soc. Am.*, 80(**1**), p. 133-145, 1986.

[18] Sumner, C. J., Lopez-Poveda, E. A, O'Mard, P., Meddis, R.: A revised model of the inner-hair cell and auditory-nerve complex, *J. Acoust. Soc. Am.*, 111(**5**), p. 2178–2188, 2002.

[19] Meddis, R.: Auditory-nerve first-spike latency and auditory absolute threshold: A computer model, *J. Acoust. Soc. Am.* 119(**1**), p. 406–417, 2006.

[20] Meddis, R.: Simulation of Mechanical to Neural Transduction in the Auditory Receptor, *J. Acoust. Soc. Am.* 79(**3**), p. 702–711, 1986.

[21] Vencovský, V.: Modeling roughness perception using a model of cochlear hydrodynamics, *Forum Acusticum 2014*, Krakow, Poland, p. 1–6, 2014.

[22] Aures, W.: *Berechnungsverfahren für den Wohlklang beliebiger Schallsignale, ein Beitrag zur gehörbezogenen Schallanalyse*, PhD thesis, TU München, 1984.

[23] Wang, Y. S.: A study on sound roughness evaluation based on an auditory synchronization index model, *Proceedings of the 2nd International Congress on Image and Signal Processing, IEEE*, p. 3612–3616, 2009.

[24] PsySound3: Sound analyses software `http://psysound.wikidot.com/`

[25] IPEM toolbox for perception-based music analysis `http://www.ipem.ugent.be/?q=node/27`

[26] Miśkiewicz, A., Majer, J.: Roughness of low-frequency pure tones and harmonic complex tones, *Forum Acusticum 2014*, Krakow, Poland, 2014.

[27] Moore, B. C. J., Glasberg, B. R., Baer, T.: A Model for the Prediction of Thresholds, Loudness, and Partial Loudness, *Journal of the Audio Engineering Society* 45(**4**), p. 224–240, 1997.

Akustické listy: ročník 20, číslo 3–4 prosinec 2014 ISSN: 1212-4702
Vydavatel: Česká akustická společnost, Technická 2, 166 27 Praha 6 Vytisklo: Nakladatelství ČVUT, výroba
Počet stran: 28 Počet výtisků: 200
Redakční rada: M. Brothánek, O. Jiříček, J. Kozák, R. Čmejla, J. Volín
Jazyková úprava: M. Tharp, R. Svobodová

Uzávěrka příštího čísla Akustických listů je 27. února 2015.